
When Policy Entropy Constraint Fails: Preserving Diversity in Flow-based RLHF via Perceptual Entropy

Xiaofeng Tan^{1,2,*} Jun Liu² Bin-Bin Gao² Yuanting Fan² Xi Jiang³
 Chengjie Wang² Hongsong Wang^{1,†} Feng Zheng^{3,†}

¹Southeast University ²Tencent Youtu Lab ³Southern University of Science and Technology
 xiaofengtan@seu.edu.cn

*Work done during Xiaofeng Tan’s internship at Tencent Youtu Lab. †Corresponding authors.

Abstract

RLHF is widely used to align flow-matching text-to-image models with human preferences, but often leads to severe diversity collapse after fine-tuning. In RL, diversity is often assumed to correlate with policy entropy, motivating entropy regularization. However, we show this intuition breaks in flow models: policy entropy remains constant, even while perceptual diversity collapses. We explain this mismatch both theoretically and empirically: the constant entropy arises from the fixed, pre-defined noise schedule, while the diversity collapse is driven by the mode-seeking nature of policy gradients. As a result, policy entropy fails to prevent the model from converging to a narrow high-reward region in the perceptual space. To this end, we introduce perceptual entropy that captures diversity in a perceptual space and maintains the property of standard entropy. Building upon this insight, we propose two entropy-regularized strategies, Perceptual Entropy Constraint and Perceptual Constraints on Generation Space, to preserve perceptual diversity and improve the quality. Experiments across two base models, neural and rule-based rewards, and three perceptual spaces demonstrate consistent gains in the quality-diversity trade-off; PEC achieves the best overall score of 0.734 (vs. baseline’s 0.366); a complementary setting of PEC further reaches a diversity average of 0.989 (vs. baseline’s 0.047). Our [project page](#) is publicly available.

1 Introduction

Flow matching [38] has emerged as a powerful paradigm for text-to-image generation [68]. Since human-centric criteria such as aesthetics [15], semantic consistency [48], and safety [42] are difficult to optimize with likelihood-based pre-training alone, recent work aligns pretrained generative models through Reinforcement Learning from Human Feedback (RLHF) [19, 40, 59].

RLHF addresses this by post-training generative models with feedback from human annotators or reward models. However, diversity can decrease during fine-tuning, which limits both (1) RLHF effectiveness and (2) real-world applicability. Specifically, (1) RLHF requires diverse and informative samples for reward evaluation; reduced diversity narrows exploration and weakens feedback scope. (2) Many applications require coverage across contexts [3, 16]. As shown in Fig. 1, Flow-GRPO produces visually similar samples for both portrait and living-room prompts, while an ideal model should preserve variations in identity, pose, background, layout, lighting, and furnishing style. This motivates us to seek RLHF frameworks that **improve quality without sacrificing diversity**.

In RL research on LLMs, diversity is commonly characterized by policy entropy [1, 11, 31, 41, 54, 79]. Under this view, recent works [12, 77] aim to balance diversity and reward \mathcal{R} using policy entropy $\exp(\mathcal{H})$, and reports an empirical relationship, $\mathcal{R} = -a \exp(\mathcal{H}) + b$, with coefficients a and b . A natural solution to diversity collapse in flow-based RLHF is therefore policy entropy regularization.

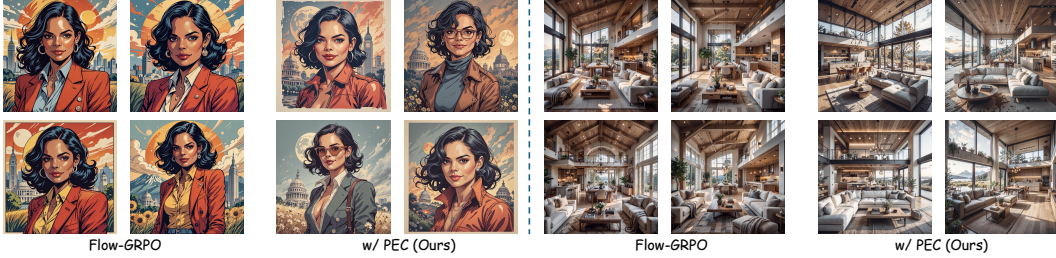


Figure 1: **Diversity Collapse.** Flow-GRPO improves quality but sacrifices diversity, producing similar styles.

However, revisiting this intuition under flow matching reveals a key inconsistency: **diversity collapses while the policy entropy surrogate remains constant**, as shown in Fig. 2. Diffusion and flow-based models [27, 55] avoid directly modeling $p(\mathbf{x}_0)$ by decomposing the process into transitions $p(\mathbf{x}_{t-1} | \mathbf{x}_t)$, which we term policy entropy. However, this quantity is fixed by the noise schedule and thus fails to reflect changes in diversity. This raises a fundamental question: *what drives diversity collapse in RL for flow models despite constant policy entropy?*

Contributions. In this paper, we investigate the diversity collapse from the perspective of entropy mechanism in flow-based RLHF, and propose a novel entropy concept with two entropy-regularization strategies to improve quality without sacrificing diversity. Main contributions are highlighted below.

First, **we investigate the apparent paradox** between constant entropy and diversity collapse in flow-based RLHF. We study two questions: (1) *why does the policy entropy remain constant after RL fine-tuning?* and (2) *why can diversity still collapse under this constant policy entropy?* (1) For the first question, we show that the noised samples \mathbf{x}_t are generated by injecting noise with a *pre-defined and fixed intensity* into the model-predicted mean $\mu_\theta(\mathbf{x}_t)$, resulting in a Gaussian distribution with fixed covariance. Hence, both likelihoods and policy entropy are determined by the fixed noise scheduler and are independent of the flow model parameters θ . (2) For the second question, we find that this paradox stems from the mode-seeking nature of online RL, where the policy is optimized to concentrate probability distribution on high-reward region in the reward space. In this case, the multi-peak pretrained policy distribution may collapse into a single-peak perceptual distribution. This motivates an RLHF framework that encourages broad coverage of multiple high-reward regions in perceptual space, rather than convergence to a single peak, as shown in Fig. 3.

Second, motivated by the observation that policy entropy in the generative space fails to capture diversity collapse, **we introduce a novel entropy concept**, *perceptual entropy* $\mathcal{H}_{\text{perc}}$, which faithfully reflects this phenomenon while remaining consistent with prior entropy-based methods. Building on this concept, we further reveal an empirical entropy-based reward for flow models, $\mathcal{R} = -a \exp(\mathcal{H}_{\text{perc}}) + b$, which is analogous to relationships observed in LLMs [12]. Furthermore, building on the above analysis, **we propose two entropy-regularized strategies** to mitigate diversity collapse: *Perceptual Entropy Constraint* (PEC), which incorporates perceptual entropy into the reward signal, and *Perceptual Constraints on Generation Space*, which aim to align the collapsed perceptual space with the consistent VAE space to maintain diversity.

Finally, comprehensive experiments on FLUX.dev [33] and SD3.5-M [18] using neural and rule-based rewards, alongside PickScore [32], DINO [8], and CLIP [48] perceptual encoders, demonstrate that perceptual entropy improves the quality-diversity trade-off: PEC achieves the best overall score of 0.734, and a complementary setting of PEC further reaches a diversity average of 0.989.

2 Preliminary

RLHF Objective and Policy Gradient. Given an external prompt condition $c \sim \mathcal{D}$ and a policy p_θ that generates $\mathbf{x} \sim p_\theta(\cdot | c)$, RLHF aims to maximize the expected reward:

$$\max_{\theta} \mathcal{J}(\theta) := \mathbb{E}_{c \sim \mathcal{D}, \mathbf{x} \sim p_\theta(\cdot | c)} [\mathcal{R}(\mathbf{x}, c)], \quad (1)$$

Considering that the gradient of the objective is difficult to estimate directly, policy gradient methods such as REINFORCE [67] decompose it into a sum of log-likelihood gradients:

$$\nabla_{\theta} \mathcal{J}(\theta) = \mathbb{E} \left[\sum_{t=1}^T \nabla_{\theta} \log p_{\theta}(\mathbf{x}_{t-1} | \mathbf{x}_t, c) \mathcal{A}(\mathbf{x}, c) \right], \quad (2)$$

where $\mathcal{A}(\mathbf{x}, c)$ denotes an advantage estimated by the final sample $\mathbf{x} \equiv \mathbf{x}_0$.

Group-Relative Advantage. GRPO [53] computes advantages via group-wise normalization. For each prompt, it samples K candidates $\{\mathbf{x}^k\}_{k=1}^K$ and normalizes rewards within the group:

$$\mathcal{A}(\mathbf{x}^i, c) = \frac{\mathcal{R}(\mathbf{x}^i, c) - \text{mean}\{\mathcal{R}(\mathbf{x}^k, c)\}}{\text{std}\{\mathcal{R}(\mathbf{x}^k, c)\}}. \quad (3)$$

Policy Density in Flow Models. For flow models, the policy in Eq. (2) is defined by the reverse-time SDE transition [19, 40]. Under the flow parameterization, each step follows a Gaussian transition

$$\mathbf{x}_{t-1} = \mu_\theta(\mathbf{x}_t, t, c) + \sigma_t \sqrt{dt} \boldsymbol{\epsilon}, \boldsymbol{\epsilon} \sim \mathcal{N}(\mathbf{0}, \mathbf{I}) \Rightarrow p_\theta(\mathbf{x}_{t-1} | \mathbf{x}_t, c) = \mathcal{N}(\mathbf{x}_{t-1}; \mu_\theta(\mathbf{x}_t, t, c), \sigma_t^2 dt \mathbf{I}), \quad (4)$$

where covariance $\sigma_t^2 dt \mathbf{I}$ is fixed by noise schedule, while mean μ_θ is given by the velocity field[40]:

$$\mu_\theta(\mathbf{x}_t, t, c) = \mathbf{x}_t + \left[v_\theta(\mathbf{x}_t, t, c) + \frac{\sigma_t^2}{2t} (\mathbf{x}_t + (1-t)v_\theta(\mathbf{x}_t, t, c)) \right] dt. \quad (5)$$

Flow-Based GRPO Objective. Flow-GRPO optimizes the policy gradient in Eq. (2) with the group-relative advantage in Eq. (3), using a clipped proximal surrogate:

$$\mathcal{J}_{\text{GRPO}}(\theta) = \mathbb{E}_{i,t} \left[\min(\rho_{t,i}(\theta) \mathcal{A}_i, \text{clip}(\rho_{t,i}(\theta), 1 - \epsilon, 1 + \epsilon) \mathcal{A}_i) \right]. \quad (6)$$

where $\rho_{t,i}(\theta) = \frac{p_\theta(\mathbf{x}_{t-1}^i | \mathbf{x}_t^i, c)}{p_{\theta_{\text{old}}}(\mathbf{x}_{t-1}^i | \mathbf{x}_t^i, c)}$ is the probability ratio between the current and old policy.

Entropy Mechanism in LLM RL. Token-level policy entropy from $p_\theta(\mathbf{x}_t | \mathbf{x}_{<t})$ is widely used for entropy regularization to encourage exploration [24, 25, 31, 54, 79, 80]. In this context, Cui et al. [12] establish an empirical relationship between policy entropy and validation reward:

$$\mathcal{R} = -a \exp(\mathcal{H}) + b, \quad (7)$$

where \mathcal{R} denotes the validation reward and $a, b > 0$ are coefficients.

3 Understanding the Failure of Policy Entropy Constraints

Entropy regularization is a standard mechanism for mitigating diversity collapse in RL. In flow-based RL, however, a direct entropy constraint on the generated-sample distribution is difficult to instantiate, motivating a closer examination of tractable entropy surrogates. We identify a paradox: *the policy entropy $\mathcal{H}(p_\theta(\mathbf{x}_{t-1} | \mathbf{x}_t, c))$ remains invariant during training, while diversity collapse still occurs.* This section analyzes this phenomenon through two questions: (1) why policy entropy remains constant during training, unlike in LLMs; and (2) why collapse still occurs despite this invariance.

3.1 From Marginal Entropy to Policy Entropy

Challenge in Estimating Marginal Entropy. In reinforcement learning, entropy regularization is typically applied to the marginal entropy $\mathcal{H}(p_\theta(\mathbf{x}_0 | c))$. In contrast, flow and diffusion models are trained through conditional transition distributions $p_\theta(\mathbf{x}_{t-1} | \mathbf{x}_t, c)$. As a result, evaluating $\mathcal{H}(p_\theta(\mathbf{x}_0 | c))$ requires access to the exact log-density of the marginal $p_\theta(\mathbf{x}_0 | c)$, which is widely recognized as an intractable issue in diffusion and flow model [9, 13, 14, 23, 45, 50, 55].

Joint Entropy & Policy Entropy. A natural alternative is to consider the entropy of the full trajectory $\mathbf{x}_{0:T}$ rather than the final sample \mathbf{x}_0 . In RL for LLMs [1, 11, 31, 41, 54, 79], the token-level policy entropy of $p_\theta(\cdot | \mathbf{x}_{<t})$ is widely used for regularization. Similarly, we consider using the policy entropy of $p_\theta(\mathbf{x}_{t-1} | \mathbf{x}_t, c)$ in flow models to obtain the joint entropy, as follows:

$$p_\theta(\mathbf{x}_{0:T} | c) = p(\mathbf{x}_T | c) \prod_{t=1}^T p_\theta(\mathbf{x}_{t-1} | \mathbf{x}_t, c) = p(\mathbf{x}_T) \prod_{t=1}^T p_\theta(\mathbf{x}_{t-1} | \mathbf{x}_t, c), \quad (\mathbf{x}_T \perp c). \quad (8)$$

Considering that the initial distribution \mathbf{x}_T follows standard Gaussian distribution $\mathcal{N}(\mathbf{0}, \mathbb{I})$, the joint entropy $\mathcal{H}(p_\theta(\mathbf{x}_{0:T} | c))$ is linearly related to the policy entropy $\mathcal{H}(p_\theta(\mathbf{x}_{t-1} | \mathbf{x}_t, c))$, as follow:

$$\mathcal{H}(p_\theta(\mathbf{x}_{0:T} | c)) = -\mathbb{E}_{p_\theta(\mathbf{x}_{0:T} | c)} [\log p(\mathbf{x}_T) + \sum_{t=1}^T \log p_\theta(\mathbf{x}_{t-1} | \mathbf{x}_t, c)] = \mathcal{H}(p(\mathbf{x}_T)) + \sum_{t=1}^T \mathcal{H}(p_\theta(\mathbf{x}_{t-1} | \mathbf{x}_t, c)).$$

where $\mathcal{H}(p(\mathbf{x}_T))$ is constant because \mathbf{x}_T is drawn from a fixed Gaussian prior.

Thus, by analogy with token-level entropy in LLMs, the policy entropy appears to be a natural tractable surrogate for trajectory-level entropy in flow-based RL. However, we observe that it is fixed by during RL fine-tuning and therefore cannot reflect the diversity collapse observed. Below, we provide the theoretical analysis in Sec. 3.2 and verify this phenomenon empirically in Fig. 2.

3.2 Constant Policy Entropy in Flow-based RL

We now formalize the per-step policy entropy induced by the reverse Gaussian transition and show that it is determined solely by the prescribed noise schedule.

Definition 1 (Policy Entropy in Flow-based RL). For a prompt $c \in \mathcal{D}$ and timestep t , the per-step conditional entropy is defined as:

$$\mathcal{H}_t(p_\theta) = -\mathbb{E}_{\{\mathbf{x}_\tau\}_{\tau=0}^T \sim p_\theta(\cdot|c)}[\log p_\theta(\mathbf{x}_{t-1} | \mathbf{x}_t, c)], \quad (9)$$

where the policy $p_\theta(\mathbf{x}_{t-1} | \mathbf{x}_t, c)$ is given by the Gaussian transition induced by the flow model θ , i.e., $\mathcal{N}(\mathbf{x}_{t-1}; \mu_\theta(\mathbf{x}_t, t, c), \sigma_t^2 dt \mathbf{I})$, defined as follows:

$$\log p_\theta(\mathbf{x}_{t-1} | \mathbf{x}_t, c) = -\frac{\|\mathbf{x}_{t-1} - \mu_\theta(\mathbf{x}_t, t, c)\|^2}{2\sigma_t^2 dt} + C_t, \quad C_t = -\frac{d}{2} \log(2\pi\sigma_t^2 dt), \quad (10)$$

where d denotes the dimensionality of \mathbf{x}_t , and C_t is constant term that is independent of θ .

Definition 1 provides the closed-form density of the policy probability and its entropy. To further analyze the quantitative property of policy entropy, we provide the following property.

Property 1 (Constant Policy Entropy in Flow-based RL). For the reverse-time transition in Eq. (4), the per-step conditional entropy at timestep t satisfies (see in App. B.1):

$$\mathcal{H}_t(p_\theta) = \frac{d}{2} - C_t. \quad (11)$$

Property 1 shows that the policy entropy is invariant to the model parameters θ and depends only on the noise schedule and dimensionality. Intuitively, variations in θ only affect the Gaussian mean $\mu_\theta(\mathbf{x}_t, t, c)$ while leaving the covariance $\sigma_t^2 dt \mathbf{I}$ unchanged. Thus, the policy entropy remains constant during model θ fine-tuning, since the covariance is fixed by the noise schedule.

Beyond the theoretical analysis, we empirically verify the constant policy entropy property in Fig. 2. As shown in Fig. 2(a), during training, the entropy and variance in the VAE space remain nearly invariant. **However, diversity in the reward-perceived space still decreases over training.** Consistent trends are also observed in the pixel and reward spaces, as shown in Fig. 2(b). Next, we analyze the underlying reason for this apparent contradiction.

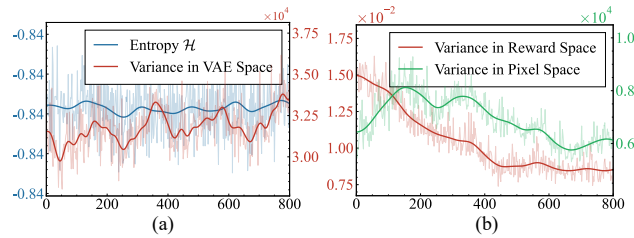


Figure 2: **Training-time Metrics.** (a) Entropy vs. variance in VAE space. (b) Variance in pixel and reward space.

3.3 Diversity Collapse behind Constant Policy Entropy

The previous section explains why entropy stays constant. We next examine why diversity can still collapse. Starting from the policy-gradient objective in Eq. (2), we present the following corollary, with proof deferred to App. B.3. This result characterizes the unclipped local policy-gradient direction underlying GRPO, rather than an exact equivalence to the full clipped GRPO surrogate.

Corollary 1 (Mode-Seeking Optimization under On-Policy Policy Gradient). For policy gradient methods [67] in Eq. (2), with $p_{\theta_{\text{old}}}$ and \mathcal{A} fixed within an update, the gradient satisfies:

$$\nabla_{\theta} \mathcal{J}(\theta) = \nabla_{\theta} \left(-D_{\text{KL}}(p_{\theta}(\mathbf{x}_{0:T}|c) \| p_{\mathcal{A}}(\mathbf{x}_{0:T}|c)) + D_{\text{KL}}(p_{\theta}(\mathbf{x}_{0:T}|c) \| p_{\theta_{\text{old}}}(\mathbf{x}_{0:T}|c)) \right),$$

where $p_{\theta}(\mathbf{x}_{0:T}|c)$ is the joint distribution, and $p_{\mathcal{A}}(\mathbf{x}_{0:T}|c)$ is the target distribution induced by advantage on the same trajectory space $p_{\mathcal{A}}(\mathbf{x}_{0:T}|c) = Z_{\mathcal{A}}(c)^{-1} p_{\theta_{\text{old}}}(\mathbf{x}_{0:T}|c) \exp(\mathcal{A}(\mathbf{x}_0, c))$ with $Z_{\mathcal{A}}(c) = \int p_{\theta_{\text{old}}}(\mathbf{x}_{0:T}|c) \exp(\mathcal{A}(\mathbf{x}_0, c)) d\mathbf{x}_{0:T}$.

Corollary 1 implies that the unclipped update direction locally minimizes the KL divergence to the advantage-induced target $p_{\mathcal{A}}$ while maximizing the KL divergence from the old policy $p_{\theta_{\text{old}}}$. The clipped GRPO objective can be viewed as a finite-sample, trust-region-style modification of this direction. Since both KL terms place p_{θ} as the first argument, they correspond to the reverse KL, which is mode-seeking [30] and drives the policy toward high-reward regions in the perceptual space while remaining close to the old policy in the generation space.

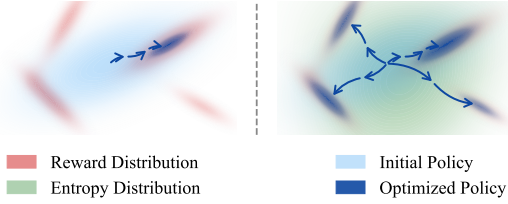


Figure 3: **Optimization Behavior.** GRPO shows mode-seeking behavior and converges to a single-peak distribution with high reward, while an ideal model should encourage coverage of multiple high-reward regions.

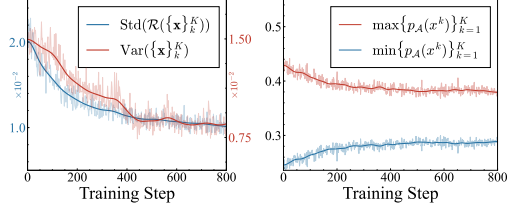


Figure 4: **Training Dynamics Metrics.** (a) variance of reward and standard deviation of samples; (b) maximum and minimum advantage probabilities p_A during training.

Conceptual Illustrations. Intuitively, the target distribution p_A is sampled from the old policy θ_{old} , and thus unexplored perceptual modes are excluded from optimization. As a result, the policy model is encouraged toward a single high-reward mode with limited coverage, leading to diversity collapse. Repeated on-policy updates therefore converge probability mass on a narrow high-reward region in the perceptual space, as shown in Fig. 3. In contrast, an ideal model augmented with a perceptual signal should promote coverage over multiple high-reward regions. Empirically, Fig. 4 shows that the dispersion of p_A decreases during training, with both reward variance and sample diversity declining, consistent with the contraction predicted by Corollary 1.

Summary. The policy entropy in the generation space remains invariant, as its covariance is fixed by the noise schedule; however, mode-seeking optimization drives the model to concentrate on a single high-reward mode with low perceptual diversity.

4 Method

In this section, we address the issue of diversity collapse. Intuitively, diversity collapse can be seen as the feature variance reduction in human perception. Our analysis above reveals a key factor: *the standard policy entropy in flow models is unable to capture this collapse*, undermining the effectiveness of existing entropy-based regularization for flow matching. This motivates us to define a new entropy concept, *perceptual entropy*, which captures diversity collapse in perceptual space while remaining consistent with existing entropy-based regularization methods.

4.1 Perceptual Entropy Proxy

To capture sample diversity via policy entropy, we introduce the concept of *perceptual entropy*. It preserves the structure of standard policy entropy but is defined in the perceptual space rather than the generative latent space, as follows.

Definition 2 (Heuristic Perceptual Entropy). Let $\phi = \mathcal{D}_{\text{vae}} \circ \mathcal{E}_p$ be a mapping where \mathcal{E}_p is a perceptual encoder and \mathcal{D}_{vae} is a VAE decoder. Given k rollout noised samples from the exploration process Eq. (4), the perceptual probability is defined as:

$$p_{\theta}^{\text{perc}}(\mathbf{x}_{t-1}^k | \mathbf{x}_t^k, c) := \mathcal{N}\left(\phi(\mathbf{x}_{t-1}^k); \phi(\mathbf{m}^k), \sigma_t^2 dt \mathbf{I}\right). \quad (12)$$

where \mathbf{m}^k denotes the old-policy mean $\mu_{\theta_{\text{old}}}(\mathbf{x}_t^k, t, c)$, and the perceptual entropy is then:

$$\mathcal{H}_{\text{perc}}(p_{\theta}) = \mathbb{E}_{t,k} \left[-\log p_{\theta}^{\text{perc}}(\mathbf{x}_{t-1}^k | \mathbf{x}_t^k, c) \right]. \quad (13)$$

Definition 2 introduces an entropy notion that quantifies diversity collapse in the perceptual space. Specifically, noised samples \mathbf{x}_t and the old-policy mean \mathbf{m}^k in the flow model are first decoded into the pixel space by a VAE decoder \mathcal{D}_{vae} , and then mapped into the perceptual space by a perceptual encoder \mathcal{E}_p . In this space, perceptual likelihoods $p_{\theta}^{\text{perc}}(\mathbf{x}_{t-1}^k | \mathbf{x}_t^k, c)$ are computed under a local Gaussian centered at $\phi(\mathbf{m}^k)$, and used to define the perceptual entropy in Eq. (13).

Perceptual Encoder. Here, we discuss the choice of perceptual encoder. For neural network-based rewards, we use the PickScore encoder to avoid additional computational cost. For rule-based rewards without an internal vision encoder, we instead adopt a frozen vision foundation model such as CLIP [48]. As discussed in Sec. 5.3 and Tab. 4, this additional perceptual encoder is both effective and efficient, yielding consistent gains with minimal overhead.

Jacobian Term. In Definition 2, the Jacobian term induced by the heterogeneous space transformation is omitted due to its computational overhead. A similar observation has been made in prior 3D generation approaches leveraging 2D priors [37, 47, 64, 66]. Following standard on-policy REINFORCE-style approximations [2, 28, 43], perceptual scores are computed on fixed old-policy rollouts and treated as shaped rewards, while the GRPO likelihood ratio handles the policy correction.

To further understand perceptual entropy, we provide a heuristic analysis of its relation to the conditional feature-space variance under a local mean-preserving approximation.

Remark 1 (Heuristic Connection to Conditional Feature-Space Variance). Let $\mathbf{z}_{t-1} = \phi(\mathbf{x}_{t-1})$. Assume that, within a local reverse step, the perceptual encoder is approximately mean-preserving, i.e., $\mathbb{E}[\mathbf{z}_{t-1} | \mathbf{x}_t] \approx \phi(\mathbf{m})$. Then perceptual entropy approximately tracks the expected conditional feature-space variance:

$$\mathcal{H}_{\text{perc}}(p_\theta) \approx \mathbb{E}_{t, \mathbf{x}_t} \left[\frac{\text{Var}(\mathbf{z}_{t-1} | \mathbf{x}_t)}{2\sigma_t^2 dt} \right] - C_t. \quad (14)$$

This Remark suggests that perceptual entropy can capture local perceptual dispersion, and is therefore aligned with existing entropy-based methods [12, 31], similar with Property 1.

Empirical Entropy Mechanism. To better understand this mechanism, we empirically study the relationship between perceptual entropy and reward in flow models, in analogy to the empirical finding in LLMs [12]. We therefore propose a similar empirical entropy mechanism for flow models:

$$\mathcal{R} = -a \exp(\mathcal{H}_{\text{perc}}) + b. \quad (15)$$

where a and b are empirical coefficients.

As shown in Fig. 5, we report the relationship between reward \mathcal{R} and perceptual entropy $\mathcal{H}_{\text{perc}}$. These results along with the theoretical analyses demonstrate that perceptual entropy provides *an effective identifier of diversity, aligning with existing research* for LLMs [12].

This naturally motivates regularizing perceptual entropy to mitigate diversity collapse. Here, we introduce two approaches based on perceptual entropy: (1) *Perceptual Entropy-Based Constraint*, which treats perceptual entropy as a principled entropy identifier and incorporates it into a standard entropy-regularization framework; and (2) *Perceptual Constraints on the VAE*, which leverages perceptual entropy to encourage consistency between the original and collapsed perceptual spaces.

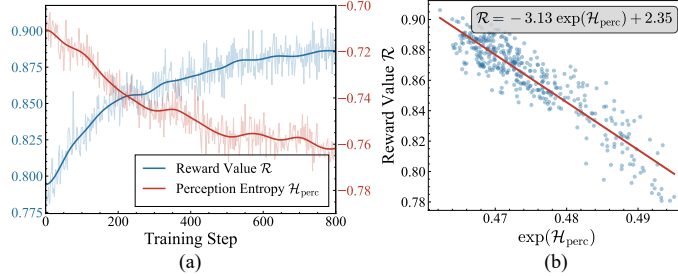


Figure 5: **Relationship between Reward and Perceptual Entropy.**

4.2 Perceptual-Regularized Strategies for GRPO

Objective. Standard RLHF inherently drives the policy toward a narrow subset of high-reward samples, thereby inducing diversity collapse. To mitigate this issue, we augment the RLHF objective in Eq. (1) with a perceptual regularization term $\Omega(p_\theta^{\text{perc}})$, as follows:

$$\max_{\theta} \mathcal{J}(\theta) = \mathbb{E}_{\mathbf{x} \sim p_\theta} [\mathcal{R}(\mathbf{x}, c)] + \lambda \Omega(p_\theta^{\text{perc}}). \quad (16)$$

Here, $\Omega(p_\theta^{\text{perc}})$ is a perceptual regularizer that encourages exploration of a broader perceptual space, while $\mathbb{E}_{\mathbf{x} \sim p_\theta} [\mathcal{R}(\mathbf{x}, c)]$ promotes high-preference samples through reward maximization.

Perceptual Entropy Constraint. Since perceptual entropy serves as a reliable surrogate for conditional variance as shown in Remark 1, a natural choice is to maximize it directly, as follows:

$$\max_{\theta} \mathcal{J}_{\text{PEC}}(\theta) = \mathbb{E}_{\mathbf{x} \sim p_\theta} [\mathcal{R}(\mathbf{x}, c)] + \lambda \mathcal{H}_{\text{perc}}(p_\theta). \quad (17)$$

Here, we set $\Omega = \mathcal{H}_{\text{perc}}(p_\theta)$ to encourage the policy to explore a broader perceptual space.

Perceptual Constraints on Generation Space. While PEC directly promotes variance, an alternative is to anchor the policy distribution to the diversity-preserving generation-space prior by setting $\Omega = -D_{\text{KL}}(p_\theta^{\text{perc}} \| p_\theta^{\text{vae}})$, as follows:

$$\max_{\theta} \mathcal{J}_{\text{PCVAE}}(\theta) = \mathbb{E}_{\mathbf{x} \sim p_\theta} [\mathcal{R}(\mathbf{x}, c)] - \lambda D_{\text{KL}}(p_\theta^{\text{perc}} \| p_\theta^{\text{vae}}). \quad (18)$$

Perceptual Reward Shaping. Although theoretically sound, optimizing PEC and PCVAE as independent auxiliary losses introduces empirical challenges. Direct entropy maximization injects unstructured stochasticity [58], leading to competing gradients against the primary reward and instability training, as shown in the red line in Fig. 6(a). To address this, we incorporate perceptual constraints directly into the reward signal, a strategy we term *perceptual reward shaping*. The shaped rewards are computed by aggregating instantaneous perceptual quantities across reverse timesteps:

$$\mathcal{J}_{\text{PEC}}(\theta) = \mathbb{E}_{c,k} \left[\underbrace{\mathcal{R}(\mathbf{x}_0^k, c) - \lambda \mathbb{E}_t \left[\log p_{\theta}^{\text{perc}}(\mathbf{x}_{t-1}^k | \mathbf{x}_t^k, c) \right]}_{\text{Shaped Reward } \tilde{\mathcal{R}}_{\text{PEC}}^k} \right]. \quad (19)$$

This incorporates perceptual constraints directly into the reward signal, ensuring that perceptual and task rewards are jointly normalized within the same GRPO rollout group, as shown by the blue line in Fig. 6(a). Similarly, the shaped reward for the PCVAE constraint is given by:

$$\tilde{\mathcal{R}}_{\text{PCVAE}}^k = \mathcal{R}(\mathbf{x}_0^k, c) - \lambda \mathbb{E}_t \left[\log p_{\theta}^{\text{perc}}(\mathbf{x}_{t-1}^k | \mathbf{x}_t^k, c) - \log p_{\theta}^{\text{vae}}(\mathbf{x}_{t-1}^k | \mathbf{x}_t^k, c) \right]. \quad (20)$$

To optimize the shaped rewards, we adopt the standard GRPO clipped surrogate, as follows:

$$\mathcal{J}_{m\text{-GRPO}}(\theta) = \mathbb{E}_{c, \{\mathbf{x}_t^k\}_{t,k}} \left[\min \left(\rho_{t,k}(\theta) \hat{\mathcal{A}}_k^m, \text{clip}(\rho_{t,k}(\theta), 1-\epsilon, 1+\epsilon) \hat{\mathcal{A}}_k^m \right) \right]. \quad (21)$$

where $\hat{\mathcal{A}}_k^m$ is the advantage in Eq.(3), and $m \in \{\text{PEC}, \text{PCVAE}\}$ denotes the constraint type.

As illustrated in Fig.6, our method effectively mitigates these optimization issues. Compared to Native KL, which introduces competing gradients, perceptual reward shaping aligns perceptual constraints with the primary objective and stabilizes training dynamics, as shown by the blue line in Fig.6(a).

Moreover, incorporating the PCVAE constraint regularizes entropy maximization, leading to higher and more stable entropy and improved output diversity, as shown in Fig. 6(b).

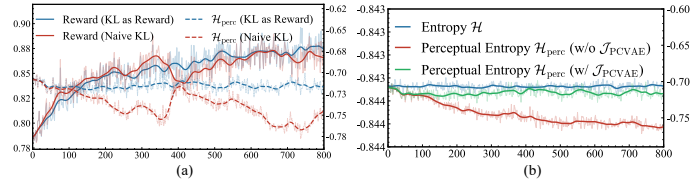


Figure 6: **Optimization Comparison.** (a) Native KL (red) versus KL-as-reward (blue), showing reward and entropy dynamics; (b) entropy with (blue) and without (red) $\mathcal{J}_{\text{PCVAE}}$.

5 Experiments

5.1 Experimental Setup

Implementation. We build upon Flow-GRPO [40] and evaluate two base models, FLUX.dev [33] and SD3.5-M [18]. For FLUX.dev, we use PickScore [32] as the neural reward and compute perceptual entropy with PickScore and DINO [8] encoders. For SD3.5-M, we follow [40] and adopt rule-based rewards, with evaluation based on CLIP [48] and DINO encoders. FLUX.dev is trained on Pick-a-Pic [32] with 37,523 prompts, and evaluated on HPD [69], while SD3.5-M is evaluated on GenEval following [40]. For PEC and PCVAE, we tune $\lambda \in \{0.03, 0.05, 0.10\}$, with larger values to encourage diversity and smaller ones for quality. All other hyperparameters kept as in Flow-GRPO [40].

Metrics. Following MixGRPO [34], we evaluate generation quality using ImageReward [72], PickScore [32], Aesthetic Predictor v2.5 [15], CLIP [48], and Unified Reward [65]. For diversity, we sample 30 outputs per prompt for 400 HPD test prompts (12,000 images per method). We report DINO and CLIP feature variances, as well as Vendi Scores [20], which measure the effective rank of the normalized similarity matrix. Vendi Scores are computed in four feature spaces: V.S._{CLIP} and V.S._{DINO} capture semantic and visual diversity in CLIP and DINO spaces, while V.S._{IR} and V.S._{PS} measure diversity in ImageReward and PickScore spaces. We further report an overall score by averaging min-max normalized quality and diversity metrics for each table.

Compared Methods. We compare standard entropy regularization [52], Clip-Higher [76], and covariance-aware Clip-Cov/KL-Cov [12]. Details are provided in App. C. We test both their original entropy terms and our perceptual entropy $\mathcal{H}_{\text{perc}}$, then compare directly with PCVAE and PEC. Hyperparameters follow Flow-GRPO unless stated otherwise: entropy weight 0.05, Clip-Cov/KL-Cov rate 0.25, Clip-Higher threshold 0.1, and KL weight 0.001 [40].

Table 1: **Entropy Regularization Comparison.** Gray-shaded rows denote our methods. Abbreviations: P.S.=PickScore, I.R.=ImageReward, U.R.=Unified Reward, and V.S.=Vendi Score.

Method	Perceptual Space	Quality \uparrow							Diversity \uparrow					Overall		
		P.S.	Aes.v2.5	I.R.	CLIP	HPSv2.1	U.R.	Norm.Avg	DINO	CLIP	V.S.CLIP	V.S.DINO	V.S.IR		V.S.PS	Norm.Avg
<i>Base Model & Baseline without Entropy Regularization</i>																
Flux Dev	-	0.226	5.837	1.089	0.388	0.312	3.540	0.000	104.76	1.11	13.45	27.05	5.73	1.47	0.753	0.376
Flow-GRPO (Baseline)	-	0.243	6.305	1.375	0.396	0.337	3.738	0.685	84.17	0.81	7.18	16.91	2.39	0.85	0.047	0.366
<i>Existing Methods with Native Entropy \mathcal{H} or Perceptual Entropy \mathcal{H}_{perc}</i>																
Flow-GRPO w/ KL	-	0.233	5.998	1.289	0.396	0.323	3.582	0.319	101.11	1.08	12.32	25.42	4.99	1.21	0.599	0.459
Clip-Higher	-	0.240	6.273	1.367	0.392	0.336	3.741	0.617	81.83	0.79	7.25	15.51	1.95	0.96	0.025	0.321
Entropy Reg.	VAE	0.240	5.965	1.362	0.398	0.332	3.615	0.473	88.32	0.94	9.15	20.02	3.29	0.97	0.247	0.360
Entropy Reg.	PickScore	0.239	6.079	1.365	0.396	0.332	3.604	0.478	96.25	1.01	10.71	25.75	4.34	1.32	0.519	0.498
Clip-Cov	VAE	0.241	6.128	1.426	0.399	0.335	3.672	0.610	89.94	0.89	10.17	17.73	3.49	1.15	0.286	0.448
Clip-Cov	PickScore	0.242	6.153	1.448	0.402	0.337	3.698	0.680	100.46	0.97	10.08	25.21	3.77	1.23	0.466	0.573
KL-Cov	VAE	0.243	6.143	1.431	0.397	0.345	3.720	0.694	94.04	0.84	8.71	17.22	2.78	0.95	0.179	0.437
KL-Cov	PickScore	0.243	6.296	1.474	0.398	0.346	3.746	0.783	96.82	0.91	9.96	23.82	3.58	1.17	0.393	0.588
<i>The Proposed Methods with Perceptual Entropy \mathcal{H}_{perc} from DINO Space</i>																
PCVAE (Ours, $\lambda = 0.03$)	DINO	0.244	6.362	1.497	0.405	0.344	3.774	0.876	92.76	0.99	9.67	20.14	3.47	1.15	0.342	0.609
PEC (Ours, $\lambda = 0.05$)	DINO	0.238	6.405	1.428	0.406	0.336	3.717	0.746	98.94	1.18	11.28	25.45	5.07	1.42	0.640	0.693
PCVAE (Ours, $\lambda = 0.10$)	DINO	0.237	6.176	1.328	0.401	0.332	3.665	0.546	118.09	1.26	12.68	27.94	6.17	1.57	0.884	0.715
PEC (Ours, $\lambda = 0.10$)	DINO	0.233	6.195	1.327	0.396	0.332	3.640	0.468	116.97	1.34	13.23	30.41	7.11	1.63	0.989	0.728
<i>The Proposed Methods with Perceptual Entropy \mathcal{H}_{perc} from PickScore Space</i>																
PCVAE (Ours, $\lambda = 0.03$)	PickScore	0.246	6.388	1.489	0.408	0.348	3.816	0.962	92.07	0.98	9.44	19.88	3.16	1.08	0.302	0.632
PCVAE (Ours, $\lambda = 0.10$)	PickScore	0.240	6.211	1.335	0.397	0.335	3.683	0.581	108.86	1.22	11.69	27.63	6.16	1.63	0.813	0.697
PEC (Ours, $\lambda = 0.05$)	PickScore	0.240	6.412	1.446	0.412	0.338	3.748	0.842	105.01	1.09	10.73	26.11	4.86	1.42	0.626	0.734
PEC (Ours, $\lambda = 0.10$)	PickScore	0.235	6.242	1.340	0.401	0.334	3.674	0.568	108.81	1.27	12.99	27.22	6.44	1.59	0.858	0.713

Table 2: **SoTA Comparison.** Type denotes post-training: N=None, U=Unknown, D=DPO, and R=reinforcement fine-tuning.

Method	Type	Quality \uparrow							Diversity \uparrow					Overall		
		PickScore	Aes.v2.5	ImageReward	CLIP	HPSv2.1	Unified Reward	Norm.Avg	DINO	CLIP	V.S.CLIP	V.S.DINO	V.S.IR		V.S.PS	Norm.Avg
SDXL [46]	N	0.226	5.836	0.980	0.411	0.294	3.410	0.205	124.96	1.20	13.7	32.4	10.1	1.48	0.937	0.571
Hunyuan-DiT [36]	U	0.224	5.659	1.080	0.406	0.303	3.428	0.190	121.73	1.09	13.8	28.7	7.38	1.35	0.763	0.476
SD-3.5-M [17]	D	0.227	5.711	1.113	0.404	0.301	3.553	0.256	115.56	1.17	12.4	28.1	6.76	1.39	0.721	0.489
Kolors [56]	N	0.225	5.994	0.977	0.385	0.314	3.362	0.143	111.80	1.05	10.8	28.3	7.01	1.31	0.601	0.372
SD-3.5-L [17]	D	0.229	5.897	1.122	0.408	0.302	3.619	0.359	123.01	1.15	12.2	27.9	6.93	1.4	0.737	0.548
HiDream-Dev [7]	U	0.229	6.049	1.329	0.398	0.325	3.781	0.527	82.55	0.88	7.92	15.8	2.57	0.94	0.039	0.283
Qwen-Image [68]	D&R	0.232	6.039	1.409	0.417	0.324	3.921	0.711	90.41	0.79	8.12	16.6	2.34	0.93	0.045	0.378
<i>Flux Dev (Base Model)</i>																
Flux Dev (Base Model)	U	0.226	5.837	1.089	0.388	0.312	3.540	0.215	104.76	1.11	13.45	27.05	5.73	1.47	0.669	0.442
PCVAE (Ours, $\lambda = 0.03$)	R	0.246	6.388	1.489	0.408	0.348	3.816	0.917	92.07	0.98	9.44	19.88	3.16	1.08	0.241	0.579
PCVAE (Ours, $\lambda = 0.10$)	R	0.240	6.211	1.335	0.397	0.335	3.683	0.645	108.86	1.22	11.69	27.63	6.16	1.63	0.727	0.686
PEC (Ours, $\lambda = 0.05$)	R	0.240	6.412	1.446	0.412	0.338	3.748	0.832	105.01	1.09	10.73	26.11	4.86	1.42	0.546	0.689
PEC (Ours, $\lambda = 0.10$)	R	0.235	6.242	1.340	0.401	0.334	3.674	0.630	108.81	1.27	12.99	27.22	6.44	1.59	0.773	0.702

5.2 Main Results

Comparison with Entropy-Based Regularization. As shown in Tab. 1, native per-step entropy \mathcal{H} provides limited gains under flow matching, whereas perceptual entropy \mathcal{H}_{perc} is more effective. Standard entropy regularization achieves an overall score of 0.360, below Flow-GRPO with KL at 0.459. Replacing \mathcal{H} with \mathcal{H}_{perc} improves the score to 0.498. Our PEC further improves performance, reaching 0.728 overall and achieving a diversity average of 0.989 in DINO perceptual space.

Comparison with SoTA Models. As shown in Tab. 2, existing text-to-image models exhibit a clear quality–diversity trade-off. SDXL achieves the highest diversity of 0.937 but a lower quality of 0.205, whereas Qwen-Image attains higher quality of 0.711 with substantially reduced diversity of 0.045. In contrast, PEC with perceptual entropy achieves the best overall score of 0.702 while maintaining strong diversity of 0.773, indicating a more favorable quality–diversity trade-off.

Trade-Off between Diversity and Quality.

Fig. 7 shows that Flow-GRPO improves quality but reduces diversity. KL alleviates this drop at a quality cost. PEC gives a better balance: $\lambda = 0.10$ preserves diversity, while $\lambda = 0.05$ keeps quality close to Flow-GRPO.

Visualization & User Study.

The teaser in Fig.1 and the extended visualizations in Fig.S1, demonstrate that PEC preserves visual diversity across prompts and domains without noticeably degrading image quality. User study details are provided in App.A.1.

5.3 Ablation Study

Effectiveness of Perceptual Entropy. Tab. 1 shows that perceptual entropy consistently improves existing methods: KL-Cov rises from 0.437 to 0.588 overall. Tab. 3 further isolates this effect in PEC, where replacing the native per-step entropy with \mathcal{H}_{perc} improves Aes.v2.5 from 6.372 to 6.412.

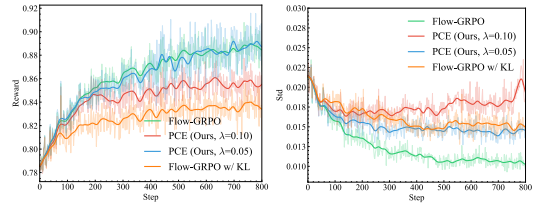


Figure 7: **Training Dynamics of Flow-GRPO, Flow-GRPO with KL, and PEC with Perceptual Entropy.** (a) Mean reward. (b) Reward standard deviation.

Table 3: **Perceptual Entropy Ablation.** Our perceptual entropy $\mathcal{H}_{\text{perc}}$ for PEC method is replaced with native entropy \mathcal{H} to examine its effectiveness.

Method	Entropy	Aes.v2.5 \uparrow	ImageReward \uparrow	CLIP \uparrow	DINO \uparrow
PEC	\mathcal{H}	6.372	1.439	0.405	89.98
PEC	$\mathcal{H}_{\text{perc}}$	6.412	1.446	0.412	105.01

Table 4: **Computational Cost.** Iteration time is normalized by Flow-GRPO. Additional cost is limited.

Method	Perceptual Encoder	Iteration Time	Peak Memory
Flow-GRPO	–	1.00 \times	78.7G
PEC (Ours)	PickScore Encoder	1.01 \times	78.7G
PEC (Ours)	DINO Encoder	1.03 \times	79.2G

Perceptual Reward Shaping vs. Native Regularization. Fig. 6 shows that perceptual reward shaping is more stable than directly optimizing the native KL or entropy regularization. This stabilizer improves quality while preserving the diversity benefit from perceptual entropy.

Perceptual Encoder. Our perceptual entropy can be computed not only with the reward model encoder, but also with a frozen DINO or CLIP encoder. As shown in Table 1, the performance gains generalize across different perceptual encoders. As shown in Table 4, the additional iteration-time overhead is marginal and peak memory usage is nearly unchanged, since the perceptual encoder is much smaller than the flow model and is evaluated asynchronously from generation and optimization.

6 Related Work

RLHF for Flow Matching. RLHF aligns generative models with human preferences via reward signals [39]. Building on early progress for diffusion models [6, 19, 59, 75], recent work extends RLHF to flow matching by enabling stochastic rollouts and GRPO-style optimization [40, 73]. Follow-up studies improve efficiency [21, 26, 35], preference modeling [78], theory [60], and reward hacking [61]. Despite these advances, RLHF for flow models often suffers from diversity collapse, and its underlying mechanism remains unclear.

Entropy in LLM Reinforcement Finetuning. Entropy is widely used to characterize exploration and predict downstream gains in RLVR [12, 25, 52]. Token-level analyses further show that high-entropy tokens often correspond to key forking points and drive a disproportionate share of learning [5, 62]. Prior work thus studies entropy-aware objectives and regularization, together with stabilizers such as loss reweighting and clip-higher, to mitigate entropy collapse [1, 11, 41, 58, 76]. In contrast, entropy in flow models can behave substantially differently, yet remains underexplored.

Entropy in Diffusion and Flow Models. Recent studies have explored entropy optimization in diffusion and flow generators under reward optimization [9, 13, 14, 22, 45, 57]. Existing approaches include variational bounds on diffusion-policy entropy [9], analytic entropy via change-of-variable formulations for flow policies [22], trajectory-level entropy-rate constraints [45], and terminal-distribution entropy maximization on the data manifold [13]. However, these methods estimate entropy in the generative space and often rely on auxiliary networks [9], theoretical approximations [14], or gradient-dependent formulations [13, 22], which limit their effectiveness in flow-based RL frameworks.

7 Conclusion

In this work, we investigate diversity collapse in flow-based RLHF from the perspective of entropy mechanism, and propose a novel perceptual entropy framework with two entropy-regularization strategies that improve alignment without sacrificing diversity. First, we identify and analyze a flow-specific paradox in which perceptual diversity collapses despite the practical policy entropy surrogate remaining nearly constant. We show that this phenomenon arises from the fixed reverse-process noise schedule, whereas diversity collapse is fundamentally driven by the mode-seeking nature of policy-gradient optimization. Second, we introduce perceptual entropy, which captures diversity in a perceptual feature space while preserving key properties of standard entropy, and further propose PEC and PCVAE to maintain perceptual diversity during reward optimization. Extensive experiments on FLUX.dev demonstrate that our method substantially improves the quality-diversity trade-off.

Limitations. This work employs GRPO as a representative RLHF framework and focuses on its application to text-to-image generation. Future work may extend this framework to other RLHF methods, such as DPO and DDPO, and broader generative modalities including video and audio.

References

- [1] Jacob Adamczyk, Volodymyr Makarenko, Stas Tiomkin, and Rahul V Kulkarni. Average-reward reinforcement learning with entropy regularization. *arXiv preprint arXiv:2501.09080*, 2025.
- [2] Arash Ahmadian, Chris Cremer, Matthias Gallé, Marzieh Fadaee, Julia Kreutzer, Olivier Pietquin, Ahmet Üstün, and Sara Hooker. Back to basics: Revisiting reinforce-style optimization for learning from human feedback in llms. In *Proceedings of the 62nd Annual Meeting of the Association for Computational Linguistics (Volume 1: Long Papers)*, pages 12248–12267, 2024.
- [3] Isabela Albuquerque, Ira Ktena, Olivia Wiles, Ivana Kajić, Amal Rannen-Triki, Cristina Vasconcelos, and Aida Nematzadeh. Benchmarking diversity in image generation via attribute-conditional human evaluation. *arXiv preprint arXiv:2511.10547*, 2025.
- [4] James Betker, Gabriel Goh, Li Jing, Tim Brooks, Jianfeng Wang, Linjie Li, Long Ouyang, Juntang Zhuang, Joyce Lee, Yufei Guo, et al. Improving image generation with better captions. *OpenAI Technical Report*, 2023.
- [5] Eric Bigelow, Ari Holtzman, Hidenori Tanaka, and Tomer Ullman. Forking paths in neural text generation. *arXiv preprint arXiv:2412.07961*, 2024.
- [6] Kevin Black, Michael Janner, Yilun Du, Ilya Kostrikov, and Sergey Levine. Training diffusion models with reinforcement learning. *arXiv preprint arXiv:2305.13301*, 2023.
- [7] Qi Cai, Jingwen Chen, Yang Chen, Yehao Li, Fuchen Long, Yingwei Pan, Zhaofan Qiu, Yiheng Zhang, Fengbin Gao, Peihan Xu, et al. Hidream-i1: A high-efficient image generative foundation model with sparse diffusion transformer. *arXiv preprint arXiv:2505.22705*, 2025.
- [8] Mathilde Caron, Hugo Touvron, Ishan Misra, Hervé Jégou, Julien Mairal, Piotr Bojanowski, and Armand Joulin. Emerging properties in self-supervised vision transformers. *CoRR*, abs/2104.14294, 2021. URL <https://arxiv.org/abs/2104.14294>.
- [9] Onur Celik, Zechu Li, Denis Blessing, Ge Li, Daniel Palenicek, Jan Peters, Georgia Chalvatzaki, and Gerhard Neumann. DIME: Diffusion-based maximum entropy reinforcement learning. In *Proceedings of the 42nd International Conference on Machine Learning*, volume 267 of *Proceedings of Machine Learning Research*, pages 6958–6977. PMLR, 13–19 Jul 2025. URL <https://proceedings.mlr.press/v267/celik25a.html>.
- [10] Xiaokang Chen, Zhiyu Wu, Xingchao Liu, Zizheng Pan, Wen Liu, Zhenda Xie, Xingkai Yu, and Chong Ruan. Janus-pro: Unified multimodal understanding and generation with data and model scaling. *arXiv preprint arXiv:2501.17811*, 2025.
- [11] Daixuan Cheng, Shaohan Huang, Xuekai Zhu, Bo Dai, Wayne Xin Zhao, Zhenliang Zhang, and Furu Wei. Reasoning with exploration: An entropy perspective. *arXiv preprint arXiv:2506.14758*, 2025.
- [12] Ganqu Cui, Yuchen Zhang, Jiacheng Chen, Lifan Yuan, Zhi Wang, Yuxin Zuo, Haozhan Li, Yuchen Fan, Huayu Chen, Weize Chen, et al. The entropy mechanism of reinforcement learning for reasoning language models. *arXiv preprint arXiv:2505.22617*, 2025.
- [13] Riccardo De Santi, Marin Vlastelica, Ya-Ping Hsieh, Zebang Shen, Niao He, and Andreas Krause. Flow density control: Generative optimization beyond entropy-regularized fine-tuning. *Advances in Neural Information Processing Systems*, 2025. URL <https://openreview.net/forum?id=ELk7sylvH7g>.
- [14] Riccardo De Santi, Marin Vlastelica, Ya-Ping Hsieh, Zebang Shen, Niao He, and Andreas Krause. Provable maximum entropy manifold exploration via diffusion models. In *Proceedings of the 42nd International Conference on Machine Learning*, volume 267 of *Proceedings of Machine Learning Research*, pages 12739–12761. PMLR, 13–19 Jul 2025. URL <https://proceedings.mlr.press/v267/de-santi25a.html>.
- [15] Discuss0434. Aesthetic-Predictor-v2-5: Siglip-based aesthetic score predictor. <https://github.com/discuss0434/aesthetic-predictor-v2-5>, 2024.
- [16] Mischa Dombrowski, Weitong Zhang, Sarah Cechnicka, Hadrien Reynaud, and Bernhard Kainz. Image generation diversity issues and how to tame them. In *Proceedings of the Computer Vision and Pattern Recognition Conference*, pages 3029–3039, 2025.
- [17] Patrick Esser, Sumith Kulal, Andreas Blattmann, Rahim Entezari, Jonas Müller, Harry Saini, Yam Levi, Dominik Lorenz, Axel Sauer, Frederic Boesel, et al. Scaling rectified flow transformers for high-resolution image synthesis. *arXiv preprint arXiv:2403.03206*, 2024.

- [18] Patrick Esser, Sumith Kulal, Andreas Blattmann, Rahim Entezari, Jonas Müller, Harry Saini, Yam Levi, Dominik Lorenz, Axel Sauer, Frederic Boesel, et al. Scaling rectified flow transformers for high-resolution image synthesis. In *International Conference on Machine Learning*, 2024.
- [19] Ying Fan, Olivia Watkins, Yuqing Du, Hao Liu, Moonkyung Ryu, Craig Boutilier, Pieter Abbeel, Mohammad Ghavamzadeh, Kangwook Lee, and Kimin Lee. Dpok: Reinforcement learning for fine-tuning text-to-image diffusion models. *Advances in Neural Information Processing Systems*, 36:79858–79885, 2023.
- [20] Dan Friedman and Adji Bousso Dieng. The vendi score: A diversity evaluation metric for machine learning. *Transactions on Machine Learning Research*, 2023.
- [21] Xiaolong Fu, Lichen Ma, Zipeng Guo, Gaojing Zhou, Chongxiao Wang, ShiPing Dong, Shizhe Zhou, Ximan Liu, Jingling Fu, Tan Lit Sin, et al. Dynamic-treerpo: Breaking the independent trajectory bottleneck with structured sampling. *arXiv preprint arXiv:2509.23352*, 2025.
- [22] Ting Gao, Stavros Orfanoudakis, Nan Lin, and Elvin Isufi. Flow matching policy with entropy regularization. *arXiv preprint arXiv:2603.17685*, 2026.
- [23] Will Grathwohl, Ricky T. Q. Chen, Jesse Bettencourt, Ilya Sutskever, and David Duvenaud. FFJORD: Free-form continuous dynamics for scalable reversible generative models. In *International Conference on Learning Representations (ICLR)*, 2019.
- [24] Tuomas Haarnoja, Haoran Tang, Pieter Abbeel, and Sergey Levine. Reinforcement learning with deep energy-based policies. In *International conference on machine learning*, pages 1352–1361. PMLR, 2017.
- [25] Tuomas Haarnoja, Aurick Zhou, Pieter Abbeel, and Sergey Levine. Soft actor-critic: Off-policy maximum entropy deep reinforcement learning with a stochastic actor. In *International conference on machine learning*, pages 1861–1870. PMLR, 2018.
- [26] Xiaoxuan He, Siming Fu, Yuke Zhao, Wanli Li, Jian Yang, Dacheng Yin, Fengyun Rao, and Bo Zhang. Tempflow-grpo: When timing matters for grpo in flow models. *arXiv preprint arXiv:2508.04324*, 2025.
- [27] Jonathan Ho, Ajay Jain, and Pieter Abbeel. Denoising diffusion probabilistic models. In *Proceedings of the 34th International Conference on Neural Information Processing Systems*, NIPS ’20, Red Hook, NY, USA, 2020. Curran Associates Inc. ISBN 9781713829546.
- [28] Jian Hu. Reinforce++: A simple and efficient approach for aligning large language models. *arXiv e-prints*, pages arXiv–2501, 2025.
- [29] Aaron Hurst, Adam Lerer, Adam P Goucher, Adam Perelman, Aditya Ramesh, Aidan Clark, AJ Ostrow, Akila Welihinda, Alan Hayes, Alec Radford, et al. Gpt-4o system card. *arXiv preprint arXiv:2410.21276*, 2024.
- [30] Haozhe Ji, Cheng Lu, Yilin Niu, Pei Ke, Hongning Wang, Jun Zhu, Jie Tang, and Minlie Huang. Towards efficient exact optimization of language model alignment. *arXiv preprint arXiv:2402.00856*, 2024.
- [31] Yuxian Jiang, Yafu Li, Guanxu Chen, Dongrui Liu, Yu Cheng, and Jing Shao. Rethinking entropy regularization in large reasoning models. *arXiv preprint arXiv:2509.25133*, 2025.
- [32] Yuval Kirstain, Adam Polyak, Uriel Singer, Shahbuland Matiana, Joe Penna, and Omer Levy. Pick-a-pic: An open dataset of user preferences for text-to-image generation. *Advances in Neural Information Processing Systems*, 36:36652–36663, 2023.
- [33] Black Forest Labs. Flux. <https://github.com/black-forest-labs/flux>, 2024.
- [34] Junzhe Li, Yutao Cui, Tao Huang, Yinping Ma, Chun Fan, Miles Yang, and Zhao Zhong. Mixgrpo: Unlocking flow-based grpo efficiency with mixed ode-sde. *arXiv preprint arXiv:2507.21802*, 2025.
- [35] Yuming Li, Yikai Wang, Yuying Zhu, Zhongyu Zhao, Ming Lu, Qi She, and Shanghang Zhang. Branchgrpo: Stable and efficient grpo with structured branching in diffusion models. *arXiv preprint arXiv:2509.06040*, 2025.
- [36] Zhimin Li, Jianwei Zhang, Qin Lin, Jiangfeng Fang, Xiaobo Wang, Wenhao Wang, Zhenyu Yang, Jiawei Li, Xianfang Shi, Hao Zhang, et al. Hunyuan-dit: A powerful multi-resolution diffusion transformer with fine-grained chinese understanding, 2024.

- [37] Chen-Hsuan Lin, Jun Gao, Luming Tang, Towaki Takikawa, Xiaohui Zeng, Xun Huang, Karsten Kreis, Sanja Fidler, Ming-Yu Liu, and Tsung-Yi Lin. Magic3d: High-resolution text-to-3d content creation. In *IEEE Conference on Computer Vision and Pattern Recognition*, 2023.
- [38] Yaron Lipman, Ricky TQ Chen, Heli Ben-Hamu, Maximilian Nickel, and Matt Le. Flow matching for generative modeling. *arXiv preprint arXiv:2210.02747*, 2022.
- [39] Buhua Liu, Shitong Shao, Bao Li, Lichen Bai, Zhiqiang Xu, Haoyi Xiong, James Kwok, Sumi Helal, and Zeke Xie. Alignment of diffusion models: Fundamentals, challenges, and future. *ACM Computing Surveys*, 2026.
- [40] Jie Liu, Gongye Liu, Jiajun Liang, Yangguang Li, Jiaheng Liu, Xintao Wang, Pengfei Wan, Di Zhang, and Wanli Ouyang. Flow-grpo: Training flow matching models via online rl. *arXiv preprint arXiv:2505.05470*, 2025.
- [41] Miao Liu, Shizhe Diao, Xiaotian Lu, Jiachen Hu, Xishan Dong, Yejin Choi, Jan Kautz, and Yuxiao Dong. Prorl: Prolonged reinforcement learning expands reasoning boundaries in large language models. *arXiv preprint arXiv:2505.24864*, 2025.
- [42] Runtao Liu, Chen I Chieh, Jindong Gu, Jipeng Zhang, Renjie Pi, Qifeng Chen, Philip Torr, Ashkan Khakzar, and Fabio Pizzati. Safetydpo: Scalable safety alignment for text-to-image generation. *arXiv preprint arXiv:2412.10493*, 2024.
- [43] Zichen Liu, Changyu Chen, Wenjun Li, Penghui Qi, Tianyu Pang, Chao Du, Wee Sun Lee, and Min Lin. Understanding rl-zero-like training: A critical perspective. *arXiv preprint arXiv:2503.20783*, 2025.
- [44] Yiyang Ma, Xingchao Liu, Xiaokang Chen, Wen Liu, Chengyue Wu, Zhiyu Wu, Zizheng Pan, Zhenda Xie, Haowei Zhang, Liang Zhao, et al. Janusflow: Harmonizing autoregression and rectified flow for unified multimodal understanding and generation. *arXiv preprint arXiv:2411.07975*, 2024.
- [45] Chika Maduabuchi. Entropy-controlled flow matching. *arXiv preprint arXiv:2602.22265*, 2026.
- [46] Dustin Podell, Zion English, Kyle Lacey, Andreas Blattmann, Tim Dockhorn, Jonas Müller, Joe Penna, and Robin Rombach. Sdxl: Improving latent diffusion models for high-resolution image synthesis. *arXiv preprint arXiv:2307.01952*, 2023.
- [47] Ben Poole, Ajay Jain, Jonathan T. Barron, and Ben Mildenhall. Dreamfusion: Text-to-3d using 2d diffusion. In *International Conference on Learning Representations*, 2023.
- [48] Alec Radford, Jong Wook Kim, Chris Hallacy, Aditya Ramesh, Gabriel Goh, Sandhini Agarwal, Girish Sastry, Amanda Askell, Pamela Mishkin, Jack Clark, et al. Learning transferable visual models from natural language supervision. In *International Conference on Machine Learning*, pages 8748–8763. PMLR, 2021.
- [49] Aditya Ramesh, Prafulla Dhariwal, Alex Nichol, Casey Chu, and Mark Chen. Hierarchical text-conditional image generation with clip latents. *arXiv preprint arXiv:2204.06125*, 2022.
- [50] Allen Z. Ren, Justin Dinh, and Hanjun Dai. Diffusion policies as an expressive policy class for offline reinforcement learning. *arXiv preprint arXiv:2408.18257*, 2024.
- [51] Robin Rombach, Andreas Blattmann, Dominik Lorenz, Patrick Esser, and Björn Ommer. High-resolution image synthesis with latent diffusion models. In *Proceedings of the IEEE/CVF Conference on Computer Vision and Pattern Recognition*, pages 10684–10695, 2022.
- [52] John Schulman, Filip Wolski, Prafulla Dhariwal, Alec Radford, and Oleg Klimov. Proximal policy optimization algorithms. *arXiv preprint arXiv:1707.06347*, 2017.
- [53] Zhihong Shao, Peiyi Wang, Qihao Zhu, Runxin Xu, Junxiao Song, Xiao Bi, Haowei Zhang, Mingchuan Zhang, Y. K. Li, Y. Wu, and Daya Guo. Deepseekmath: Pushing the limits of mathematical reasoning in open language models, 2024. URL <https://arxiv.org/abs/2402.03300>.
- [54] Wei Shen, Guanlin Liu, Zheng Wu, Ruofei Zhu, Qingping Yang, Chao Xin, Yu Yue, and Lin Yan. Exploring data scaling trends and effects in reinforcement learning from human feedback. *arXiv preprint arXiv:2503.22230*, 2025.
- [55] Yang Song, Jascha Sohl-Dickstein, Diederik P. Kingma, Abhishek Kumar, Stefano Ermon, and Ben Poole. Score-based generative modeling through stochastic differential equations. In *International Conference on Learning Representations*, 2021. URL <https://openreview.net/forum?id=PXTIG12RRHS>.

- [56] Kolors Team. Kolors: Effective training of diffusion model for photorealistic text-to-image synthesis. *Technical report*, 2024. URL <https://github.com/Kwai-Kolors/Kolors/>. Project release; no arXiv identifier is listed in the official repository.
- [57] Masatoshi Uehara, Yulai Zhao, Tommaso Biancalani, and Sergey Levine. Understanding reinforcement learning-based fine-tuning of diffusion models: A tutorial and review. *arXiv preprint arXiv:2407.13734*, 2024.
- [58] Abdullah Vanlioglu. Entropy-guided sequence weighting for efficient exploration in rl-based llm fine-tuning. *arXiv preprint arXiv:2503.22456*, 2025.
- [59] Bram Wallace, Meihua Dang, Rafael Rafailov, Linqi Zhou, Aaron Lou, Senthil Purushwalkam, Stefano Ermon, Caiming Xiong, Shafiq Joty, and Nikhil Naik. Diffusion model alignment using direct preference optimization. In *Proceedings of the IEEE/CVF Conference on Computer Vision and Pattern Recognition*, pages 8228–8238, 2024.
- [60] Feng Wang and Zihao Yu. Coefficients-preserving sampling for reinforcement learning with flow matching. *arXiv preprint arXiv:2509.05952*, 2025.
- [61] Jing Wang, Jiajun Liang, Jie Liu, Henglin Liu, Gongye Liu, Jun Zheng, Wanyuan Pang, Ao Ma, Zhenyu Xie, Xintao Wang, et al. Grpo-guard: Mitigating implicit over-optimization in flow matching via regulated clipping. *arXiv preprint arXiv:2510.22319*, 2025.
- [62] Shenzhi Wang, Le Yu, Chang Gao, Chuji Zheng, Shixuan Liu, Rui Lu, Kai Dang, Xionghui Chen, Jianxin Yang, Zhenru Zhang, et al. Beyond the 80/20 rule: High-entropy minority tokens drive effective reinforcement learning for llm reasoning. *arXiv preprint arXiv:2506.01939*, 2025.
- [63] Xinlong Wang, Xiaosong Zhang, Zhengxiong Luo, Quan Sun, Yufeng Cui, Jinsheng Wang, Fan Zhang, Yuezhe Wang, Zhen Li, Qiying Yu, et al. Emu3: Next-token prediction is all you need. *arXiv preprint arXiv:2409.18869*, 2024.
- [64] Xinzhou Wang, Yikai Wang, Junliang Ye, Fuchun Sun, Zhengyi Wang, Ling Wang, Pengkun Liu, Kai Sun, Xintong Wang, Fangfu Liu, and Bin He. Animatabledreamer: Text-guided non-rigid 3d model generation and reconstruction with canonical score distillation. In *European Conference on Computer Vision*, 2024.
- [65] Yibin Wang, Yuhang Zang, Hao Li, Cheng Jin, and Jiaqi Wang. Unified reward model for multimodal understanding and generation. *arXiv preprint arXiv:2503.05236*, 2025.
- [66] Zhengyi Wang, Cheng Lu, Yikai Wang, Fan Bao, Chongxuan Li, Hang Su, and Jun Zhu. Prolicfdreamer: High-fidelity and diverse text-to-3d generation with variational score distillation. In *Advances in Neural Information Processing Systems*, 2023.
- [67] Ronald J Williams. Simple statistical gradient-following algorithms for connectionist reinforcement learning. *Machine learning*, 8:229–256, 1992.
- [68] Chenfei Wu, Jiahao Li, Jingren Zhou, An Yang, Bin Bai, Bo Zhang, Bowen Zheng, Bowen Yu, Chengpeng Chen, Dayiheng Huang, et al. Qwen-image technical report, 2025.
- [69] Xiaoshi Wu, Yiming Hao, Keqiang Sun, Yixiong Chen, Feng Zhu, Rui Zhao, and Hongsheng Li. Human preference score v2: A solid benchmark for evaluating human preferences of text-to-image synthesis. *arXiv preprint arXiv:2306.09341*, 2023.
- [70] Enze Xie, Junsong Chen, Yuyang Zhao, Jincheng Yu, Ligeng Zhu, Yujun Lin, Zhekai Zhang, Muyang Li, Junyu Chen, Han Cai, et al. Sana 1.5: Efficient scaling of training-time and inference-time compute in linear diffusion transformer. *arXiv preprint arXiv:2501.18427*, 2025.
- [71] Jinheng Xie, Weijia Mao, Zechen Bai, David Junhao Zhang, Weihao Wang, Kevin Qinghong Lin, Yuchao Gu, Zhijie Chen, Zhenheng Yang, and Mike Zheng Shou. Show-o: One single transformer to unify multimodal understanding and generation. *arXiv preprint arXiv:2408.12528*, 2024.
- [72] Jiazheng Xu, Xiao Liu, Yuchen Wu, Yuxuan Tong, Qinkai Li, Ming Ding, Jie Tang, and Yuxiao Dong. Imagereward: Learning and evaluating human preferences for text-to-image generation. *Advances in Neural Information Processing Systems*, 36:15903–15935, 2023.
- [73] Zeyue Xue, Jie Wu, Yu Gao, Fangyuan Kong, Lingting Zhu, Mengzhao Chen, Zhiheng Liu, Wei Liu, Qiushan Guo, Weilin Huang, et al. Dancegrpo: Unleashing grpo on visual generation. *arXiv preprint arXiv:2505.07818*, 2025.

- [74] Zhiyuan Yan, Junyan Ye, Weijia Li, Zilong Huang, Shenghai Yuan, Xiangyang He, Kaiqing Lin, Jun He, Conghui He, and Li Yuan. Gpt-imgeval: A comprehensive benchmark for diagnosing gpt-4o in image generation. *arXiv preprint arXiv:2504.02782*, 2025.
- [75] Kai Yang, Jian Tao, Jiafei Lyu, Chunjiang Ge, Jiabin Chen, Weihang Shen, Xiaolong Zhu, and Xiu Li. Using human feedback to fine-tune diffusion models without any reward model. In *Proceedings of the IEEE/CVF Conference on Computer Vision and Pattern Recognition*, pages 8941–8951, 2024.
- [76] Qiyang Yu, Zheng Zhang, Ruofei Zhu, Yufeng Yuan, Xiaochen Zuo, Yu Yue, Weinan Dai, Tiantian Fan, Gaohong Liu, Lingjun Liu, et al. Dapo: An open-source llm reinforcement learning system at scale. *arXiv preprint arXiv:2503.14476*, 2025.
- [77] Yang Yue, Zhiqi Chen, Rui Lu, Andrew Zhao, Zhaokai Wang, Shiji Song, and Gao Huang. Does reinforcement learning really incentivize reasoning capacity in llms beyond the base model? *arXiv preprint arXiv:2504.13837*, 2025.
- [78] Kaiwen Zheng, Huayu Chen, Haotian Ye, Haoxiang Wang, Qinsheng Zhang, Kai Jiang, Hang Su, Stefano Ermon, Jun Zhu, and Ming-Yu Liu. Diffusionnft: Online diffusion reinforcement with forward process. *arXiv preprint arXiv:2509.16117*, 2025.
- [79] Xinyu Zhu, Mengzhou Xia, Zhepei Wei, Wei-Lin Chen, Danqi Chen, and Yu Meng. The surprising effectiveness of negative reinforcement in llm reasoning, 2025. *arXiv preprint arXiv:2506.01347*, 2025.
- [80] Brian D Ziebart, Andrew L Maas, J Andrew Bagnell, Anind K Dey, et al. Maximum entropy inverse reinforcement learning. In *AAAI*, volume 8, pages 1433–1438. Chicago, IL, USA, 2008.

When Policy Entropy Constraint Fails: Preserving Diversity in Flow-based RLHF via Perceptual Entropy

Supplementary Material

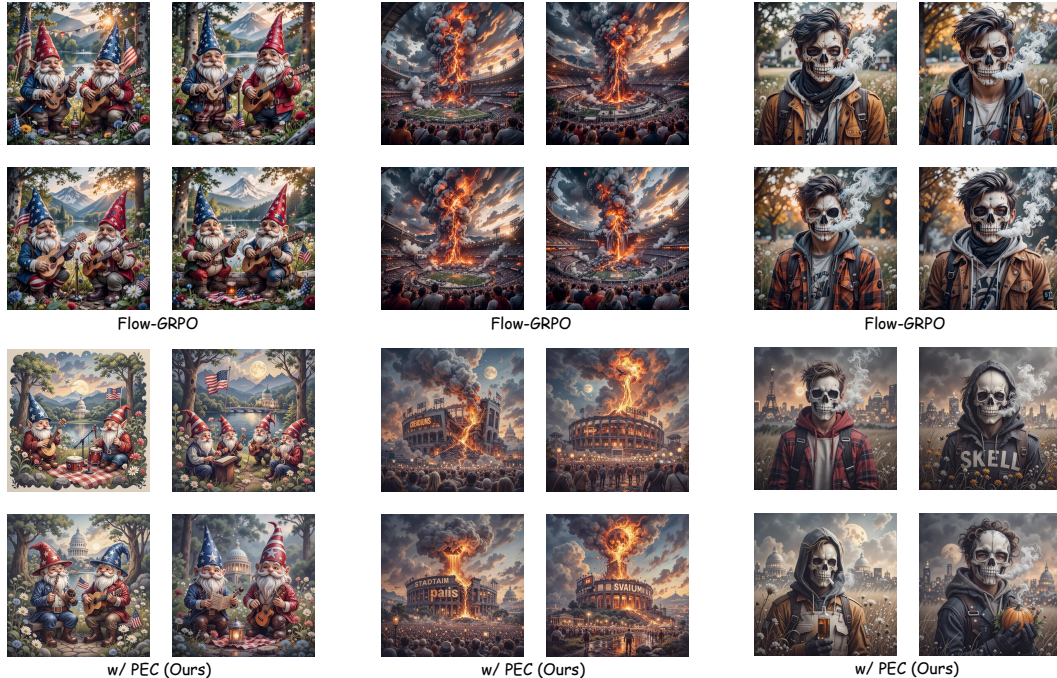


Figure S1: **Extended Diversity Visualization.** PEC preserves visible variation across prompts and visual domains.

This supplementary document presents additional experimental results, including extended visualizations in Sec.A.1, user studies in Sec.A.1, and reward variance analysis in Sec.A.2. It further provides supporting derivations and heuristic discussions in Sec.B, followed by implementation details of covariance-aware entropy control in Sec. C.

A Experiments

A.1 Extended Visualization and User Study

Our method demonstrates strong diversity preservation across diverse prompts and domains. Fig. S1 presents an extensive collection of generated images showcasing the diversity of our approach. PEC effectively balances quality and diversity: images maintain high aesthetic and semantic quality while exhibiting substantial visual variation within each prompt category, demonstrating that our perceptual entropy constraint successfully mitigates diversity collapse.

To further validate the effectiveness of our approach, we conduct a user study comparing our PEC method with Flow-GRPO. The study follows a blind, randomized, side-by-side protocol: participants are shown two anonymized image sets generated by the two methods in random order and are asked to choose the better set, or indicate no clear preference, under three criteria: overall preference, diversity, and quality. We collect 100 annotations over 20 unique image-set pairs. Specifically, we recruited 20 volunteer participants from graduate students and researchers familiar with text-to-image generation. Each participant annotated five randomized image-set pairs, yielding five independent annotations per unique pair. As shown in Fig. S2, PEC is preferred over Flow-GRPO in 64% of overall judgments and 82% of diversity judgments, with 20% and 10% no-preference responses, respectively. For image quality, participants rate the two methods comparably, with 38% preferring PEC, 43% preferring Flow-GRPO, and 19% indicating no clear preference. The results demonstrate that our perceptual

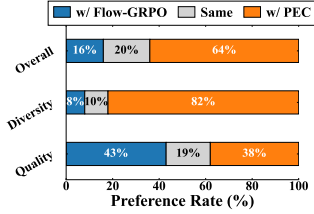


Figure S2: User Study Preferences.

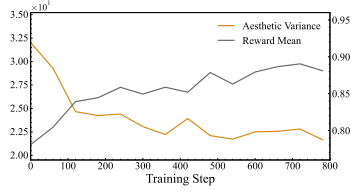


Figure S3: Aesthetic Space Variance.

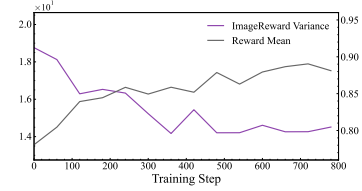


Figure S4: ImageReward Space Variance.

Table S1: **GenEval Result.** Results for models other than SD3.5-M are from [74] or the corresponding original papers. Obj.: Object; Attr.: Attribute binding.

Model	Overall	Single Obj.	Two Obj.	Counting	Colors	Position	Attr. Binding
<i>Diffusion Models</i>							
LDM [51]	0.37	0.92	0.29	0.23	0.70	0.02	0.05
SD1.5 [51]	0.43	0.97	0.38	0.35	0.76	0.04	0.06
SD2.1 [51]	0.50	0.98	0.51	0.44	0.85	0.07	0.17
SD-XL [46]	0.55	0.98	0.74	0.39	0.85	0.15	0.23
DALLE-2 [49]	0.52	0.94	0.66	0.49	0.77	0.10	0.19
DALLE-3 [4]	0.67	0.96	0.87	0.47	0.83	0.43	0.45
<i>Autoregressive Models</i>							
Show-o [71]	0.53	0.95	0.52	0.49	0.82	0.11	0.28
Emu3-Gen [63]	0.54	0.98	0.71	0.34	0.81	0.17	0.21
JanusFlow [44]	0.63	0.97	0.59	0.45	0.83	0.53	0.42
Janus-Pro-7B [10]	0.80	0.99	0.89	0.59	0.90	0.79	0.66
GPT-4o [29]	0.84	0.99	0.92	0.85	0.92	0.75	0.61
<i>Flow Matching Models</i>							
FLUX.1 Dev [33]	0.66	0.98	0.81	0.74	0.79	0.22	0.45
SD3.5-L [18]	0.71	0.98	0.89	0.73	0.83	0.34	0.47
SANA-1.5 4.8B [70]	0.81	0.99	0.93	0.86	0.84	0.59	0.65
SD3.5-M [18]	0.63	0.98	0.78	0.50	0.81	0.24	0.52
SD3.5-M+Flow-GRPO	0.95	1.00	0.99	0.95	0.92	0.99	0.86
+PEC (Ours)	0.97	1.00	0.99	0.97	0.94	1.00	0.91

entropy constraint improves subjective diversity and overall preference while maintaining comparable image quality.

A.2 Reward Variance Analysis on Other Perceptual Spaces

To verify that our findings generalize beyond the default perceptual space, we analyze reward variance dynamics in alternative perceptual spaces defined by the Aesthetic and ImageReward encoders. As shown in Figs. S3 and S4, the same diversity-quality trade-off pattern emerges across different perceptual spaces: vanilla Flow-GRPO progressively reduces reward variance during training, reflecting the implicit drive toward mode collapse identified in our theoretical analysis. These results confirm that the entropy-variance relationship established in our framework is not an artifact of a particular feature space but a general property of flow-based RLHF. Runtime overhead and DINO entropy-space results have been moved to the main text (Sec. 5.3, Tab. 4, and Tab. 1).

A.3 Rule-Based Reward Results on SD3.5-M

To complement the FLUX.dev experiments with neural rewards, we further consider the rule-based reward setting used in Flow-GRPO [40]. For completeness, Tab. S1 reproduces the GenEval comparison table from Flow-GRPO and includes our PEC variant under the same SD3.5-M family setting. Tab. S2 reports the corresponding diversity metrics. Taken together, these results show that perceptual entropy improves instruction-following performance while preserving diversity: PEC achieves higher GenEval performance than SD3.5-M+Flow-GRPO and obtains the best diversity average among the SD3.5-M variants.

Table S2: **Diversity Comparison on SD3.5-M.** Here, perceptual entropy is computed with a frozen CLIP encoder.

Method	DINO	CLIP	V.S. _{CLIP}	V.S. _{DINO}	V.S. _{IR}	V.S. _{PS}	Norm.Avg
SD3.5-M	115.56	1.17	<u>12.40</u>	<u>28.10</u>	6.76	1.41	0.801
SD3.5-M+Flow-GRPO	87.22	0.89	7.30	15.75	2.46	0.78	0.000
PCVAE	118.63	1.26	11.68	27.02	<u>6.85</u>	<u>1.48</u>	<u>0.822</u>
PEC	126.03	1.41	12.44	28.58	7.82	1.58	1.000

B Supporting Derivations and Heuristic Discussions

B.1 Proof of Property 1

In this section, we establish Property 1: under the reverse transition in Sec. 2, per-step conditional entropy is independent of θ . We restate the claim for convenience.

Property (Constant Per-step Entropy in Flow-based RL). For the reverse-time transition defined in Eq. (4), the per-step conditional entropy at timestep t satisfies:

$$\mathcal{H}_t(p_\theta) = \frac{d}{2} - C_t.$$

where d is the dimension of \mathbf{x}_t , and C_t is a constant depending on timestep t .

Proof. By substituting Eqs. (4) and the log-probability definition into Eq. (9), the following key property can be derived.

We analyze the entropy term $\mathcal{H}(p_\theta) = -\mathbb{E}_{p_\theta}[\log p_\theta]$ in the gradient computation. To simplify the analysis, we directly consider sampling from p_θ .

For a continuous Gaussian transition $p_\theta(\mathbf{x}_{t-1}|\mathbf{x}_t, c)$ at fixed timestep t , the per-step conditional entropy is

$$\mathcal{H}_t(p_\theta) = -\mathbb{E}_{\mathbf{x}_{t-1}, \mathbf{x}_t}[\log p_\theta(\mathbf{x}_{t-1}|\mathbf{x}_t, c)]. \quad (\text{S1})$$

Since $p_\theta(\mathbf{x}_{t-1}|\mathbf{x}_t, c) = \mathcal{N}(\mu_\theta(\mathbf{x}_t, t), \sigma_t^2 dt \mathbf{I})$, we have $\mathbf{x}_{t-1} = \mu_\theta(\mathbf{x}_t, t) + \sigma_t \sqrt{dt} \cdot \epsilon$ where $\epsilon \sim \mathcal{N}(\mathbf{0}, \mathbf{I})$.

The log-probability is:

$$\log p_\theta(\mathbf{x}_{t-1}|\mathbf{x}_t, c) = -\frac{\|\mathbf{x}_{t-1} - \mu_\theta(\mathbf{x}_t, t)\|^2}{2\sigma_t^2 dt} + C_t \quad (\text{S2})$$

Substituting the sampling formula $\mathbf{x}_{t-1} = \mu_\theta(\mathbf{x}_t, t) + \sigma_t \sqrt{dt} \cdot \epsilon$ gives

$$\log p_\theta(\mathbf{x}_{t-1}|\mathbf{x}_t, c) = -\frac{\|\sigma_t \sqrt{dt} \cdot \epsilon\|^2}{2\sigma_t^2 dt} + C_t = -\frac{\|\epsilon\|^2}{2} + C_t. \quad (\text{S3})$$

Taking the expectation over $\epsilon \sim \mathcal{N}(\mathbf{0}, \mathbf{I})$ yields

$$\mathcal{H}_t(p_\theta) = -\mathbb{E}_\epsilon \left[-\frac{\|\epsilon\|^2}{2} + C_t \right] = \mathbb{E}_\epsilon \left[\frac{\|\epsilon\|^2}{2} \right] - C_t = \frac{d}{2} - C_t. \quad (\text{S4})$$

where we used $\mathbb{E}[\|\epsilon\|^2] = d$. Here $\|\epsilon\|^2$ follows a chi-squared distribution $\chi^2(d)$ with d degrees of freedom, so its mean is d .

Therefore, we conclude:

$$\boxed{\mathcal{H}_t(p_\theta) = \frac{d}{2} - C_t} \quad (\text{S5})$$

This completes the proof. □

B.2 Proof of Latent-Space Conditional Variance Interpretation

In this section, we connect the per-step entropy $\mathcal{H}(p_\theta)$ in flow matching to the expected conditional variance of sampled latent variables \mathbf{x}_{t-1} given \mathbf{x}_t . Consistent with prior work [40, 73], \mathbf{x} refers to samples in the flow model’s latent space rather than images in pixel space. We use $\text{Var}(\mathbf{x}_{t-1} | \mathbf{x}_t)$ as a shorthand for the scalar $\text{tr}(\text{Cov}(\mathbf{x}_{t-1} | \mathbf{x}_t))$, i.e., the (sum of marginal) conditional variance of \mathbf{x}_{t-1} given \mathbf{x}_t . We restate the claim formally as a Lemma.

Lemma (Conditional Variance Interpretation of Per-Step Entropy). *For the reverse-time Gaussian transition in Eq. (4), the per-step entropy in flow matching satisfies*

$$\mathcal{H}(p_\theta) = \mathbb{E}_{t, \mathbf{x}_t} \left[\frac{\text{Var}(\mathbf{x}_{t-1} | \mathbf{x}_t)}{2\sigma_t^2 dt} \right] - C,$$

where C is a constant independent of θ .

Proof. We begin by analyzing the entropy of the conditional distribution $p_\theta(\mathbf{x}_{t-1} | \mathbf{x}_t, c)$. The derivation follows the same approach as Property 1. Recall that

$$p_\theta(\mathbf{x}_{t-1} | \mathbf{x}_t, c) = \mathcal{N}(\mathbf{x}_{t-1}; \mu_\theta(\mathbf{x}_t, t), \sigma_t^2 dt \cdot \mathbf{I}), \quad (\text{S6})$$

with the corresponding log-probability

$$\log p_\theta(\mathbf{x}_{t-1} | \mathbf{x}_t, c) = -\frac{\|\mathbf{x}_{t-1} - \mu_\theta(\mathbf{x}_t, t)\|^2}{2\sigma_t^2 dt} + C. \quad (\text{S7})$$

The differential entropy is then

$$\mathcal{H}(p_\theta) = -\mathbb{E}_{\mathbf{x}_{t-1}, \mathbf{x}_t, t} [\log p_\theta(\mathbf{x}_{t-1} | \mathbf{x}_t, c)] = \mathbb{E}_{\mathbf{x}_{t-1}, \mathbf{x}_t, t} \left[\frac{\|\mathbf{x}_{t-1} - \mu_\theta(\mathbf{x}_t, t)\|^2}{2\sigma_t^2 dt} \right] - C. \quad (\text{S8})$$

Recall from Eq. (4) that $\mathbf{x}_{t-1} = \mu_\theta(\mathbf{x}_t, t) + \sigma_t \sqrt{dt} \epsilon$ with $\epsilon \sim \mathcal{N}(\mathbf{0}, \mathbf{I})$, so the conditional mean is

$$\bar{\mathbf{x}}_{t-1} := \mathbb{E}[\mathbf{x}_{t-1} | \mathbf{x}_t] = \mu_\theta(\mathbf{x}_t, t). \quad (\text{S9})$$

Plugging this in and pulling the inner expectation through, we obtain

$$\mathcal{H}(p_\theta) = \mathbb{E}_{t, \mathbf{x}_t} \left[\frac{1}{2\sigma_t^2 dt} \mathbb{E}_{\mathbf{x}_{t-1} | \mathbf{x}_t} [\|\mathbf{x}_{t-1} - \bar{\mathbf{x}}_{t-1}\|^2] \right] - C. \quad (\text{S10})$$

By definition, the expected squared deviation from the conditional mean is the trace of the conditional covariance, which equals the (sum of marginal) conditional variance:

$$\mathbb{E}_{\mathbf{x}_{t-1} | \mathbf{x}_t} [\|\mathbf{x}_{t-1} - \bar{\mathbf{x}}_{t-1}\|^2] = \text{tr}(\text{Cov}(\mathbf{x}_{t-1} | \mathbf{x}_t)) = \text{Var}(\mathbf{x}_{t-1} | \mathbf{x}_t). \quad (\text{S11})$$

Substituting back and absorbing the time-step expectation gives the claimed identity:

$$\boxed{\mathcal{H}(p_\theta) = \mathbb{E}_{t, \mathbf{x}_t} \left[\frac{\text{Var}(\mathbf{x}_{t-1} | \mathbf{x}_t)}{2\sigma_t^2 dt} \right] - C.} \quad (\text{S12})$$

This completes the proof. \square

B.3 Proof of Corollary 1

We first restate the corollary to be proven, then provide the detailed proof.

Corollary (Mode-Seeking Optimization under On-Policy Policy Gradient). *For policy gradient methods [67] in Eq. (2), with $p_{\theta_{\text{old}}}$ and \mathcal{A} fixed within an update, the gradient satisfies:*

$$\nabla_\theta \mathcal{J}(\theta) = \nabla_\theta \left(-D_{\text{KL}}(p_\theta(\cdot | c) \| p_{\mathcal{A}}(\cdot | c)) + D_{\text{KL}}(p_\theta(\cdot | c) \| p_{\theta_{\text{old}}}(\cdot | c)) \right),$$

where all distributions are over trajectories $\mathbf{x}_{0:T}$, and $p_{\mathcal{A}}(\mathbf{x}_{0:T} | c) = Z_{\mathcal{A}}(c)^{-1} p_{\theta_{\text{old}}}(\mathbf{x}_{0:T} | c) \exp(\mathcal{A}(\mathbf{x}_0, c))$ with $Z_{\mathcal{A}}(c) = \int p_{\theta_{\text{old}}}(\mathbf{x}_{0:T} | c) \exp(\mathcal{A}(\mathbf{x}_0, c)) d\mathbf{x}_{0:T}$.

Proof. Starting from the trajectory-level REINFORCE policy gradient in Eq. (2):

$$\nabla_\theta \mathcal{J}(\theta) = \mathbb{E}_{\mathbf{x}_{0:T} \sim p_\theta(\cdot | c)} \left[\mathcal{A}(\mathbf{x}_0, c) \sum_{t=1}^T \nabla_\theta \log p_\theta(\mathbf{x}_{t-1} | \mathbf{x}_t, c) \right]. \quad (\text{S13})$$

Using the trajectory factorization

$$\log p_\theta(\mathbf{x}_{0:T} | c) = \log p(\mathbf{x}_T) + \sum_{t=1}^T \log p_\theta(\mathbf{x}_{t-1} | \mathbf{x}_t, c), \quad (\text{S14})$$

and taking ∇_θ on both sides, the noise prior $p(\mathbf{x}_T)$ is independent of θ so $\nabla_\theta \log p(\mathbf{x}_T) = 0$. This gives

$$\nabla_\theta \log p_\theta(\mathbf{x}_{0:T}|c) = \sum_{t=1}^T \nabla_\theta \log p_\theta(\mathbf{x}_{t-1}|\mathbf{x}_t, c). \quad (\text{S15})$$

Therefore:

$$\nabla_\theta \mathcal{J}(\theta) = \mathbb{E}_{\mathbf{x}_{0:T} \sim p_\theta} [\mathcal{A}(\mathbf{x}_0, c) \nabla_\theta \log p_\theta(\mathbf{x}_{0:T}|c)]. \quad (\text{S16})$$

We rewrite $\mathcal{A}(\mathbf{x}_0, c)$ as a log-density. Note that the naive Boltzmann form $p_{\mathcal{A}} \propto \exp(\mathcal{A}(\mathbf{x}_0, c))$ on the trajectory space is not a proper density: since \mathcal{A} depends only on the terminal \mathbf{x}_0 , $\int \exp(\mathcal{A}(\mathbf{x}_0, c)) d\mathbf{x}_{0:T}$ factors through an unbounded integral $\int 1 d\mathbf{x}_{1:T} = \infty$ over the intermediate variables and diverges. Using $p_{\theta_{\text{oid}}}$ as the base measure (as in the corollary) supplies a normalized density on $\mathbf{x}_{1:T}$ and makes $p_{\mathcal{A}}$ a valid probability distribution:

$$p_{\mathcal{A}}(\mathbf{x}_{0:T}|c) = \frac{1}{Z_{\mathcal{A}}(c)} p_{\theta_{\text{oid}}}(\mathbf{x}_{0:T}|c) \exp(\mathcal{A}(\mathbf{x}_0, c)). \quad (\text{S17})$$

Inverting this definition gives

$$\mathcal{A}(\mathbf{x}_0, c) = \log p_{\mathcal{A}}(\mathbf{x}_{0:T}|c) - \log p_{\theta_{\text{oid}}}(\mathbf{x}_{0:T}|c) + \log Z_{\mathcal{A}}(c). \quad (\text{S18})$$

Substituting Eq. (S18) into Eq. (S16):

$$\begin{aligned} \nabla_\theta \mathcal{J}(\theta) &= \mathbb{E}_{p_\theta} [\log p_{\mathcal{A}} \nabla_\theta \log p_\theta] - \mathbb{E}_{p_\theta} [\log p_{\theta_{\text{oid}}} \nabla_\theta \log p_\theta] \\ &\quad + \log Z_{\mathcal{A}}(c) \cdot \mathbb{E}_{p_\theta} [\nabla_\theta \log p_\theta]. \end{aligned} \quad (\text{S19})$$

(S20)

The third term vanishes by the score-function identity $\mathbb{E}_{p_\theta} [\nabla_\theta \log p_\theta] = \nabla_\theta \mathbb{E}_{p_\theta} [1] = 0$.

We now apply the log-derivative trick in reverse, which requires the integrand to be θ -independent. Here $\log p_{\theta_{\text{oid}}}$ is fixed by construction; for $\log p_{\mathcal{A}}$, the partition function $Z_{\mathcal{A}}(c) = \mathbb{E}_{\mathbf{x}_{0:T} \sim p_{\theta_{\text{oid}}}(\cdot|c)} [\exp(\mathcal{A}(\mathbf{x}_0, c))]$ is an expectation under the frozen rollout policy and is therefore independent of θ (had it been taken under p_θ , the trick would acquire an extra $-\nabla_\theta \log Z_{\mathcal{A}}(c) \neq 0$ correction). Both terms thus satisfy

$$\mathbb{E}_{p_\theta} [\log p_{\mathcal{A}} \nabla_\theta \log p_\theta] = \nabla_\theta \mathbb{E}_{p_\theta} [\log p_{\mathcal{A}}], \quad \mathbb{E}_{p_\theta} [\log p_{\theta_{\text{oid}}} \nabla_\theta \log p_\theta] = \nabla_\theta \mathbb{E}_{p_\theta} [\log p_{\theta_{\text{oid}}}] \quad (\text{S21})$$

Hence

$$\nabla_\theta \mathcal{J}(\theta) = \nabla_\theta \mathbb{E}_{p_\theta} [\log p_{\mathcal{A}} - \log p_{\theta_{\text{oid}}}] \quad (\text{S22})$$

Adding and subtracting $\log p_\theta$ inside each expectation yields the standard cross-entropy / KL identities:

$$\mathbb{E}_{p_\theta} [\log p_{\mathcal{A}}] = -D_{\text{KL}}(p_\theta \| p_{\mathcal{A}}) - \mathcal{H}(p_\theta), \quad \mathbb{E}_{p_\theta} [\log p_{\theta_{\text{oid}}}] = -D_{\text{KL}}(p_\theta \| p_{\theta_{\text{oid}}}) - \mathcal{H}(p_\theta). \quad (\text{S23})$$

Subtracting cancels the entropy and gives

$$\mathbb{E}_{p_\theta} [\log p_{\mathcal{A}} - \log p_{\theta_{\text{oid}}}] = -D_{\text{KL}}(p_\theta \| p_{\mathcal{A}}) + D_{\text{KL}}(p_\theta \| p_{\theta_{\text{oid}}}). \quad (\text{S24})$$

Combining with Eq. (S22) yields the final gradient formula:

$$\boxed{\nabla_\theta \mathcal{J}(\theta) = \nabla_\theta \left(-D_{\text{KL}}(p_\theta(\cdot|c) \| p_{\mathcal{A}}(\cdot|c)) + D_{\text{KL}}(p_\theta(\cdot|c) \| p_{\theta_{\text{oid}}}(\cdot|c)) \right)}. \quad (\text{S25})$$

This completes the proof. \square

B.4 Heuristic Derivation for Remark 1

We do not view this subsection as a formal proof. Instead, it provides a first-order derivation that motivates Remark 1 in the main text, showing why perceptual entropy can behave like a conditional feature-space variance score under a local approximation. This is intended as a local conditional interpretation, rather than an exact characterization of total cross-sample variance. As in the main text, we use $\text{Var}(\mathbf{z} | \mathbf{x})$ as a shorthand for $\text{tr}(\text{Cov}(\mathbf{z} | \mathbf{x}))$, the (sum of marginal) conditional variance of \mathbf{z} given \mathbf{x} . We restate the claim for convenience.

Remark (Heuristic Connection to Conditional Feature-Space Variance). Let $\mathbf{z}_{t-1} = \phi(\mathbf{x}_{t-1})$ and $\mathbf{m} = \mu_{\theta_{\text{oid}}}(\mathbf{x}_t)$ as in Definition 2, with all expectations conditioned on \mathbf{x}_t taken under the

rollout transition $p_{\theta_{\text{old}}}$. Assume that, within a local reverse step, the perceptual encoder is approximately mean-preserving, i.e., $\mathbb{E}[\mathbf{z}_{t-1} | \mathbf{x}_t] \approx \phi(\mathbf{m})$. Then the perceptual entropy in Definition 2 approximately tracks the expected conditional feature-space variance:

$$\mathcal{H}_{\text{perc}}(p_{\theta}) \approx \mathbb{E}_{t, \mathbf{x}_t} \left[\frac{\text{Var}(\mathbf{z}_{t-1} | \mathbf{x}_t)}{2\sigma_t^2 dt} \right] - C_t,$$

where $C_t = -\frac{d}{2} \log(2\pi\sigma_t^2 dt)$ is independent of θ .

Heuristic derivation. Local linearization of ϕ . Under the rollout transition, $\mathbf{x}_{t-1} | \mathbf{x}_t \sim \mathcal{N}(\mathbf{m}, \sigma_t^2 dt \mathbf{I})$ with $\mathbf{m} = \mu_{\theta_{\text{old}}}(\mathbf{x}_t)$, so \mathbf{m} is exactly the conditional mean of \mathbf{x}_{t-1} given \mathbf{x}_t . For a frozen encoder ϕ , the second-order Taylor expansion around \mathbf{m} gives

$$\phi(\mathbf{x}_{t-1}) = \phi(\mathbf{m}) + J_{\phi}(\mathbf{m})(\mathbf{x}_{t-1} - \mathbf{m}) + \frac{1}{2}(\mathbf{x}_{t-1} - \mathbf{m})^{\top} H_{\phi}(\mathbf{m})(\mathbf{x}_{t-1} - \mathbf{m}) + \mathcal{O}(\|\mathbf{x}_{t-1} - \mathbf{m}\|^3). \quad (\text{S26})$$

Since $\mathbb{E}[\mathbf{x}_{t-1} - \mathbf{m} | \mathbf{x}_t] = \mathbf{0}$ holds exactly under $p_{\theta_{\text{old}}}$, the first-order term vanishes upon taking expectations. The leading residual is a second-order Jensen gap:

$$\mathbb{E}_{\mathbf{x}_{t-1} | \mathbf{x}_t} [\phi(\mathbf{x}_{t-1})] = \phi(\mathbf{m}) + \frac{1}{2} \sigma_t^2 dt \text{tr}(H_{\phi}(\mathbf{m})) + \mathcal{O}((\sigma_t^2 dt)^2). \quad (\text{S27})$$

When the encoder is locally smooth, i.e., $\sigma_t^2 dt \|H_{\phi}\|$ is small, this yields the mean-preserving approximation $\mathbb{E}[\phi(\mathbf{x}_{t-1}) | \mathbf{x}_t] \approx \phi(\mathbf{m})$.

Perceptual entropy as a conditional residual term. Starting from Definition 2, the perceptual entropy proxy is

$$\mathcal{H}_{\text{perc}}(p_{\theta}) = \mathbb{E}_{t, k} \left[-\log p_{\theta}^{\text{perc}}(\mathbf{z}_{t-1}^k | \mathbf{x}_t^k, c) \right], \quad (\text{S28})$$

where $\mathbf{z}_{t-1} = \phi(\mathbf{x}_{t-1})$ denotes samples in the perceptual space. We treat p_{θ}^{perc} as a feature-space scoring distribution, not as an exact density obtained by a change of variables, and therefore omit the Jacobian of ϕ . This follows the same convention as score distillation and related variants, in which a frozen diffusion or vision model supplies a surrogate optimization signal without modeling the full Jacobian of the external mapping [37, 47, 64, 66].

Under the Gaussian score in Definition 2, p_{θ}^{perc} has mean $\phi(\mathbf{m})$ and isotropic covariance $\sigma_t^2 dt \cdot \mathbf{I}$ (which omits the Jacobian factor $J_{\phi} J_{\phi}^{\top}$ present in the exact pushforward covariance, consistent with the surrogate-scoring convention stated above), so its log-density is

$$\log p_{\theta}^{\text{perc}} = -\frac{\|\mathbf{z}_{t-1} - \phi(\mathbf{m})\|^2}{2\sigma_t^2 dt} + C, \quad C = -\frac{d}{2} \log(2\pi\sigma_t^2 dt). \quad (\text{S29})$$

Taking the negative expectation, the perceptual entropy proxy at fixed t becomes

$$\mathcal{H}_{\text{perc}}(p_{\theta} | t) = \frac{1}{2\sigma_t^2 dt} \mathbb{E}_{\mathbf{x}_t} \mathbb{E}_{\mathbf{z}_{t-1} | \mathbf{x}_t} [\|\mathbf{z}_{t-1} - \phi(\mathbf{m})\|^2] - C. \quad (\text{S30})$$

Approximation to conditional variance. Combining the mean-preserving result $\mathbb{E}[\mathbf{z}_{t-1} | \mathbf{x}_t] = \phi(\mathbf{m}) + \mathcal{O}(\sigma_t^2 dt)$ with the bias-variance decomposition

$$\mathbb{E}[\|\mathbf{z}_{t-1} - \phi(\mathbf{m})\|^2 | \mathbf{x}_t] = \text{tr}(\text{Cov}(\mathbf{z}_{t-1} | \mathbf{x}_t)) + \|\mathbb{E}[\mathbf{z}_{t-1} | \mathbf{x}_t] - \phi(\mathbf{m})\|^2,$$

the bias term is $\mathcal{O}((\sigma_t^2 dt)^2)$ and is negligible when the encoder is locally smooth, yielding

$$\mathbb{E}_{\mathbf{z}_{t-1} | \mathbf{x}_t} [\|\mathbf{z}_{t-1} - \phi(\mathbf{m})\|^2] \approx \text{tr}(\text{Cov}(\mathbf{z}_{t-1} | \mathbf{x}_t)) = \text{Var}(\mathbf{z}_{t-1} | \mathbf{x}_t). \quad (\text{S31})$$

Substituting back and taking the expectation over timesteps yields

$$\boxed{\mathcal{H}_{\text{perc}}(p_{\theta}) \approx \mathbb{E}_{t, \mathbf{x}_t} \left[\frac{\text{Var}(\mathbf{z}_{t-1} | \mathbf{x}_t)}{2\sigma_t^2 dt} \right] - C_t}, \quad (\text{S32})$$

which shows that perceptual entropy tracks the conditional feature-space variance of the reverse transition up to a timestep-dependent affine transformation.

For a rollout group $\{\mathbf{z}_{t-1}^k\}_{k=1}^K = \{\phi(\mathbf{x}_{t-1}^k)\}_{k=1}^K$, the corresponding empirical proxy at timestep t centers each residual at the rollout-policy transition mean $\phi(\mathbf{m}^k)$ with $\mathbf{m}^k = \mu_{\theta_{\text{old}}}(\mathbf{x}_t^k, t, c)$:

$$\widehat{\text{Var}}(t) = \frac{1}{K} \sum_{k=1}^K \|\mathbf{z}_{t-1}^k - \phi(\mathbf{m}^k)\|^2, \quad (\text{S33})$$

which gives a sample estimate of $\mathbb{E}_{\mathbf{x}_t} [\text{Var}(\mathbf{z}_{t-1} | \mathbf{x}_t)]$ used in the reward shaping of Sec. 4.2. \square

C Covariance-Aware Entropy Control for Flow GRPO

Natural policy gradient is rarely used in post-training of generative models due to its second-order optimization cost. However, its target formulation with KL constraints shares the same spirit with TRPO and PPO. Motivated by the log-probability-advantage covariance principle discussed in prior LLM RL analyses [12], we construct a flow analogue for GRPO using reverse-transition likelihoods and derive covariance-aware constraints.

C.1 Covariance-Based Sample Identification

For a batch of N transitions $\{(\mathbf{x}_{t-1}^i, \mathbf{x}_t^i, c^i)\}_{i=1}^N$ sampled from the exploration stage, we measure how strongly the log-probability and advantage co-vary for each sample. Specifically, for each transition i , we compute the centered cross-product:

$$\text{Cov}(i) = \left(\log p_\theta(\mathbf{x}_{t-1}^i | \mathbf{x}_t^i, c^i) - \bar{\ell} \right) \cdot (\mathcal{A}_i - \bar{\mathcal{A}}), \quad (\text{S34})$$

where $\bar{\ell} = \frac{1}{N} \sum_{j=1}^N \log p_\theta(\mathbf{x}_{t-1}^j | \mathbf{x}_t^j, c^j)$ is the batch mean log-probability and $\bar{\mathcal{A}} = \frac{1}{N} \sum_{j=1}^N \mathcal{A}_j$ is the batch mean advantage. Here, $p_\theta(\mathbf{x}_{t-1} | \mathbf{x}_t, c^i) = \mathcal{N}(\mu_\theta(\mathbf{x}_t, t, c^i), \sigma_t^2 \mathbf{I})$ is the conditional Gaussian policy with log-probability $\log p_\theta(\mathbf{x}_{t-1} | \mathbf{x}_t, c^i) = -\frac{\|\mathbf{x}_{t-1} - \mu_\theta(\mathbf{x}_t, t, c^i)\|^2}{2\sigma_t^2 dt} + C_t$, and \mathcal{A}_i denotes the GRPO group-normalized advantage. The empirical covariance in Eq. (S34) instantiates the analogous covariance between transition log-likelihood and advantage in the flow setting.

A large positive $\text{Cov}(i)$ indicates that transitions with high log-probability receive high advantages (and vice versa), signaling a strong positive correlation between policy likelihood and performance. Following the same covariance interpretation, such transitions are treated as entropy-reducing samples during gradient optimization. The key insight is that by identifying and selectively moderating updates on these high-covariance samples, we can control the rate of entropy collapse while maintaining reward optimization.

C.2 Entropy-Aware Constraint via Gradient Clipping

The Clip-Cov strategy leverages covariance scores to selectively suppress entropy-accelerating gradients. Given covariance bounds $\omega_{\text{low}}, \omega_{\text{high}} \in \mathbb{R}$ and a clipping ratio $r \in (0, 1)$, we randomly select transitions whose covariance falls within the specified range:

$$\mathcal{I}_{\text{clip}} \sim \text{Uniform}\left(\{i \mid \text{Cov}(i) \in [\omega_{\text{low}}, \omega_{\text{high}}]\}, \lfloor r \cdot N \rfloor\right). \quad (\text{S35})$$

The Clip-Cov objective then detaches these selected transitions from gradient flow:

$$\mathcal{J}_{\text{Clip-Cov}}(\theta) = \mathcal{J}_{\text{GRPO}}(\theta) \mathbf{1}_{\{i \notin \mathcal{I}_{\text{clip}}\}}. \quad (\text{S36})$$

By zeroing out gradients on transitions with covariance in $[\omega_{\text{low}}, \omega_{\text{high}}]$, we prevent the most aggressive entropy-reducing updates while preserving normal gradient flow on the majority of the batch. This achieves a pragmatic balance: entropy-accelerating samples are suppressed, but the policy still makes meaningful progress on reward optimization. The clipping ratio r and covariance bounds $\omega_{\text{low}}, \omega_{\text{high}}$ serve as tunable parameters to control the strength of entropy regularization. In practice, ω_{high} is typically set to a very large value (effectively $+\infty$) since we aim to suppress the most aggressive entropy-reducing updates. For simplicity, we directly select the top 25% of transitions with the largest $\text{Cov}(i)$ as the clipping set $\mathcal{I}_{\text{clip}}$.

Integrating Perceptual Entropy into Clip-Cov. To incorporate perceptual entropy $\mathcal{H}_{\text{perc}}$ into the Clip-Cov framework, we replace the standard covariance computation with a perceptual covariance metric. Specifically, we compute the perceptual log-probability $\log p_{\text{perc}}(\mathbf{x}_{t-1}^i | \mathbf{x}_t^i, c^i)$ for each generated sample, and define the perceptual covariance as:

$$\text{Cov}_{\text{perc}}(i) = \left(\log p_{\text{perc}}(\mathbf{x}_{t-1}^i | \mathbf{x}_t^i, c^i) - \bar{\ell}_{\text{perc}} \right) \cdot (\mathcal{A}_i - \bar{\mathcal{A}}), \quad (\text{S37})$$

where $\bar{\ell}_{\text{perc}} = \frac{1}{N} \sum_{j=1}^N \log p_{\text{perc}}(\mathbf{x}_{t-1}^j | \mathbf{x}_t^j, c^j)$ is the mean perceptual log-probability and $\bar{\mathcal{A}} = \frac{1}{N} \sum_{j=1}^N \mathcal{A}_j$ is the batch mean advantage. Transitions with large $\text{Cov}_{\text{perc}}(i)$ indicate samples that achieve high advantage yet receive high perceptual likelihood, signaling potential diversity collapse in perceptual space. The modified Clip-Cov objective then selects samples based on $\text{Cov}_{\text{perc}}(i)$ instead of $\text{Cov}(i)$, thereby directly targeting perceptual diversity preservation.

C.3 Entropy-Aware Constraint via KL Regularization

An alternative approach applies a reverse-KL penalty directly to high-covariance transitions. Given a threshold ratio $k \in (0, 1)$ and penalty strength $\beta > 0$, we identify the top- k proportion of transitions ranked by covariance:

$$\mathcal{I}_{\text{KL}} = \left\{ i \mid \text{Rank}(\text{Cov}(i)) \leq k \cdot N \right\}, \quad (\text{S38})$$

where $\text{Rank}(\text{Cov}(i))$ denotes the rank in descending covariance order. For these entropy-critical transitions, we impose a reverse-KL constraint:

$$\mathcal{J}_{\text{KL-Cov}}(\theta) = \mathcal{J}_{\text{GRPO}}(\theta) - \beta D_{\text{KL}}(p_{\theta_{\text{old}}}(\mathbf{x}_{t-1}^i \mid \mathbf{x}_t^i, c^i) \parallel p_{\theta}(\mathbf{x}_{t-1}^i \mid \mathbf{x}_t^i, c^i)) \mathbf{1}_{\{i \in \mathcal{I}_{\text{KL}}\}}. \quad (\text{S39})$$

For Gaussian policies with shared covariance $\sigma_t^2 dt$, this KL divergence reduces to:

$$D_{\text{KL}}(p_{\theta_{\text{old}}} \parallel p_{\theta}) = \frac{\|\mu_{\theta_{\text{old}}}^i - \mu_{\theta}^i\|^2}{2\sigma_t^2 dt}. \quad (\text{S40})$$

The KL-Cov approach penalizes large policy changes on entropy-critical samples, thereby constraining the magnitude of entropy-reducing updates. The penalty coefficient β governs the trade-off between reward optimization and entropy preservation. In contrast to Clip-Cov, which discretely suppresses gradients, KL-Cov applies a continuous penalty that allows some flexibility while still dampening aggressive updates. Together, these two strategies provide complementary mechanisms to moderate entropy decrease by directly targeting samples identified as entropy accelerators through the flow covariance criterion.

Integrating Perceptual Entropy into KL-Cov. To integrate perceptual entropy into the KL-Cov framework, we replace the sample ranking criterion with perceptual covariance. Instead of ranking by $\text{Cov}(i)$, we identify the top- k proportion of transitions ranked by perceptual covariance:

$$\mathcal{I}_{\text{KL-perc}} = \left\{ i \mid \text{Rank}(\text{Cov}_{\text{perc}}(i)) \leq k \cdot N \right\}, \quad (\text{S41})$$

where $\text{Rank}(\text{Cov}_{\text{perc}}(i))$ denotes the rank in descending perceptual covariance order. The modified objective applies the same KL penalty to these selected transitions:

$$\mathcal{J}_{\text{KL-Cov-perc}}(\theta) = \mathcal{J}_{\text{GRPO}}(\theta) - \beta D_{\text{KL}}(p_{\theta_{\text{old}}}(\mathbf{x}_{t-1}^i \mid \mathbf{x}_t^i, c^i) \parallel p_{\theta}(\mathbf{x}_{t-1}^i \mid \mathbf{x}_t^i, c^i)) \mathbf{1}_{\{i \in \mathcal{I}_{\text{KL-perc}}\}}. \quad (\text{S42})$$

By selecting samples based on perceptual covariance, the KL penalty is applied to transitions that most strongly contribute to perceptual entropy decrease, thereby directly targeting diversity preservation in perceptual space.

D Broader Impact

Positive impacts. This work improves diversity preservation in RLHF-aligned text-to-image generation, enabling models to produce a broader range of high-quality outputs for a given prompt. This benefits creative applications such as design assistance, content creation, and personalized media generation, where coverage across diverse styles and contexts is essential.

Negative impacts. Improved image generation quality and diversity may lower the barrier to producing misleading or harmful visual content, including deepfakes and synthetic disinformation. This is a general concern shared by all advances in generative modeling. We note that our method is a fine-tuning technique applied on top of existing models (FLUX.dev) that already carry their own usage policies, and we do not release new model weights at this time.